Chapter 1

Introduction

In recent years, wireless communications in the microwave and millimeter wave ranges play a very important role in our daily life because many of the military-controlled channels are now released to the commercial systems. The deregulation of the communication services also results in the rapid development of many wireless communications systems for voice and data transmissions. Multi-channel transmission with multiple operating frequencies to increase the transmission capacity is a common practice used for signal transmission in modern wireless communication. Nevertheless, when the operating frequencies of the system are more than two and the neighboring frequencies are located closely to each other, the device used in this system will produce intermodulation distortion. Consequently, for the device used in the wireless communication, it is important not only to reduce the noise power but also to level down the nonlinear distortion caused by the devices to minimize the degradation of the signal-to-noise ratio (SNR) of the system during signal transmission. Therefore, the device needs to be carefully choosing and designed to reduce the noise figure (NF) and improve the linearity.

Compound semiconductor devices offer superior performance over Si-based counterparts especially in low noise and high power applications. Among them, GaAs high electron mobility transistors (HEMTs) offer best low noise performance over others. In the HEMT structure, the specific epitaxial layers are designed to generate a band-gap discontinuity and produce two dimensional electron gas (2DEG) regions in the channel as shown in Fig.1-1. The electrons confined in the 2DEG regions result in less electron-impurity scattering and causes enhanced electron mobility, which enables HEMT to have a low noise figure meanwhile possesses high power density,

high efficiency and good linearity. In the modern digital wireless communication systems, low noise HEMTs with high linearity are required. In recent years, many works on HEMT device linearity improvement were reported. These include analysis of device linearity by nonlinearity circuit [1-2], and improvement of device linearity using double-heterojunction [3], doped-channel [4] and different device structure designs [5]. In this study, we investigate the device linearity improvement for the low noise GaAs HEMT using device layer structure and doping profile modifications.

Based on the fact that device gain compression is caused mainly by the cubic term of the Taylor expansion. The third-order intermodulation distortion (IM3) and the third-order intercept point (IP3) are the important specifications for the device linearity. Drain-Source current model and a simple device equivalent circuit were used for device linearity analysis and the derivation of the relationships between IM3 and IP3 with the two current source Gm (V_{GS}) and Gds (V_{DS}) are described in Chapter 2. To further investigate the linearity performance of the devices, polynomial curve fitting technique was applied on the transfer characteristic functions of these devices. According to the linearity analysis, four types of device structures were proposed with flat Gm distribution for device linearity improvement in this thesis. They are composite-channel MHEMT, delta doped and uniform doped MHEMT, channel doped InGaP HEMT and Schottky layer doped InGaP HEMT.

The details of the metamorphic high electron mobility transistor (MHEMT) and the pseudomorphic high electron mobility transistor (PHEMT) processes are described in Chapter 3. Device linearity improvement analysis is discussed in Chapter 4 to Chapter 7. Chapter 4 describes the device performance of the MHEMTs. Chapter 5 compares the device performance of MHEMTs with two different types of doping (δ doped and uniformly-doped). The electrical characteristics of the InGaP/AlGaAs/InGaAs PHEMT are investigated in Chapter 6. The HEMT device

structure was designed with AlGaAs spacer to improve the device noise and linearity. Chapter 7 studies the InGaP PHEMT with doping profile modification for linearity improvement. The δ doped InGaP/InGaAs PHEMTs with doping modification in the Schottky layer and in the channel region was designed to reduce IM3 for linearity improvement. In this chapter, it is demonstrated that the channel doped device has the best linearity performance compared to the other profiles studied. Finally, the work on device linearity improvements in this thesis is summarized in Chapter 8 as the conclusions.

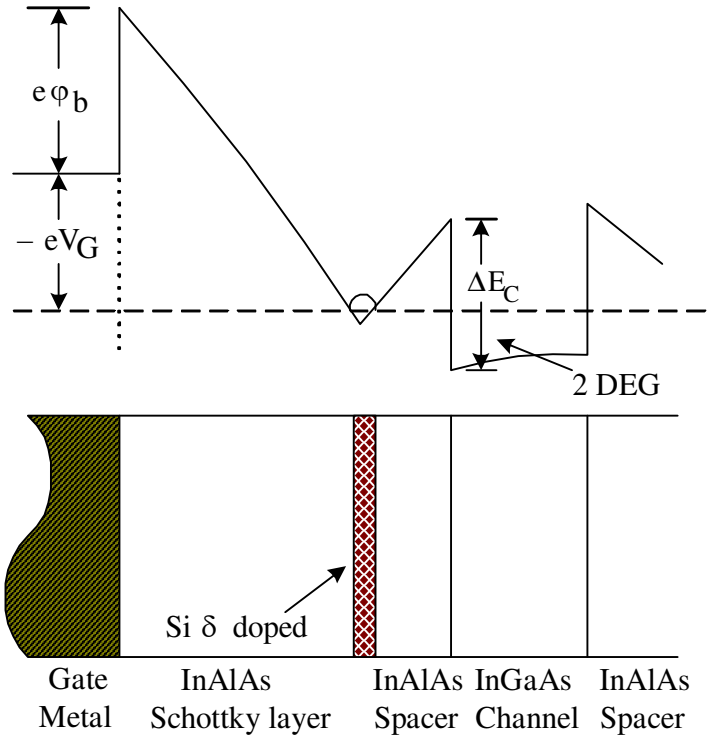

Figure 1-1 The band diagram of the InAlAs/InGaAs MHEMT.

Chapter 2

Device Linearity Analysis

2.1 Introduction

For wireless communication system, the signal was transmitted and received by the transceiver. In ideal linear and noiseless situation, transmitted signal can be recovered at the receiver. However, in real transceivers, nonlinear devices generate nonlinear distortion. The nonlinear effects of the device include gain compression and intermodulation distortion.

2.2 The nonlinear effects of device

2.2.1 Gain compression

We observed device nonlinear phenomena with a single frequency input as shown in equation (2.1):

$$v_i = A\cos\omega t \tag{2.1}$$

The nonlinear voltage gain of devices may be approximated by the polynomial expansion as equation (2.2):

$$v_o = k_1 v_i + k_2 v_i^2 + k_3 v_i^3 \tag{2.2}$$

To substitute equation (2.1) into (2.2), many of the nonlinearities may be observed.

$$\begin{aligned} v_o = {} & 0.5A^2 k_2 + \left(k_1 A + 0.75 k_3 A^3\right)\cos\omega_1 t + 0.5 k_2 A^2 \cos 2\omega_1 t \\ & + 0.25 k_3 \cos 3\omega_1 t + .. \end{aligned} \tag{2.3}$$

Equation (2.3) shows one collects the terms of the series expansion, the nonlinear phenomena of output include a shift in the DC level ($0.5A^2k_2$), gain compression ($k_1A+0.75k_3A^3$) and harmonics. The gain compression with increasing signal level is due to the cubic term which has to be negative to account for gain compression, and

not gain expansion. The second harmonic is caused by the square term, k_2 and the third harmonics are caused by the cubic term, k_3.

2.2.2 Analysis of IM3 and IP3

In modern wireless communication system, multi-channel transmission is a common practice used for signal transmission. The transmission bandwidth of communication system was divided into multiple information bandwidths and used multiple operating frequencies for data transmission to increase the transmission capacity. Nevertheless, when the operating frequencies of the system are more than two and the neighboring frequencies are located closely to each other, the device used in such system will generate intermodulation distortion.

For the intermodulation distortion analysis, two-tone signal which consists of two signals with the same amplitude A at two different but closely located frequencies is applied as the input. Substitution of the two-tone input signal as shown in equation (2.4) into equation (2.2), the output voltage is as shown in equation (2.5).

$$v_i = A\cos\omega_1 t + A\cos\omega_2 t \tag{2.4}$$

$$\begin{aligned} v_o = {} & k_1 A^2 \cos(\omega_1 - \omega_2)t + \left(k_1 A + 2.25k_3 A^3\right)\cos\omega_1 t + \left(k_1 A + 2.25k_3 A^3\right)\cos\omega_2 t \\ & + 0.75k_3 A^3 \cos(2\omega_1 - \omega_2)t + 0.75k_3 A^3 \cos(2\omega_2 - \omega_1)t \\ & + k_2 A^2 \cos(\omega_1 + \omega_2) + 0.5k_2 A^2 \cos 2\omega_1 t + 0.5k_2 A^2 \cos 2\omega_2 t \\ & + 0.75k_3 A^3 \cos(2\omega_1 + \omega_2)t + 0.75k_3 A^3 \cos(2\omega_2 + \omega_1)t \\ & + 0.25k_3 \cos 3\omega_1 t + 0.25k_3 A^3 \cos 3\omega_2 t + .. \end{aligned} \tag{2.5}$$

Among all the intermodulation distortions incurred by the devices, because of gain compression is caused mainly by the cubic tear, third-order intermodulation distortion (IM3) and the third-order intercept point (IP3) will dominate and determine the device linearity. Therefore, IM3 and IP3 have become the important figure of merit for the devices used for modern wireless communication applications. In this

chapter, IM3 and IP3 were as the device linearity specification and derivative the relationships between IM3 and IP3 with two current source parameter Gm (V_{GS}) and Gds (V_{DS}).

The IM3 level at frequencies $(2\omega_1 - \omega_2)$ and $(2\omega_2 - \omega_1)$ are as equation (2.6) [1]:

$$v_{o(IM3)} = 0.75k_3A^3\cos(2\omega_1 - \omega_2)t + 0.75k_3A^3\cos(2\omega_2 - \omega_1)t \quad (2.6)$$

An illustration of the output power spectrum is shown in Fig.2-1.

For device linearity improvement, a simple device equivalent circuit as shown in Fig. 2 was used to derivate the relationship between IM3, IP3 and Gm. The nonlinear circuit elements involved in this model are the Schottky-barrier junction capacitance at the gate (C_{gs}), the gate to drain capacitance (C_{gd}), the intrinsic transconductance (g_m) and the drain conductance (G_d). Among them, C_{gs} and g_m are dependent on the input voltage (V_i), and Gd is dependent on the output voltage (V_o) [2]. Analysis and estimation of the IM3 level and IP3 incurred by the device itself begin with the derivation of the nonlinear transfer function of the two-port network using classical theory [1]. In such case, the device may be classified as near-linear two-port system with a relatively small amount of nonlinearity. The two-port's voltage gain may then be approximated by the polynomial expansion as: (2.2):

Applying Kirchhoff's Current Law (KCL) and Kirchhoff's Voltage Law (KVL) at specific nodes of the network, the nonlinear voltage transfer function can be derived:

$$v_o = \left[\frac{j\omega C_{gd}}{G_d} - \frac{g_m}{G_d}\right]\cdot\left[1 + \frac{j\omega C_{gd}}{G_d}\right]^{-1} v_i \quad (2.7)$$

Considering the first order significant terms for simplicity of analysis, the coefficients in equation (2.7) can be expressed explicitly as $k_1 = -g_m/G_d$, $k_2 = -g_m'/G_d$ and $k_3 = -(1/2)\,g_m''/G_d$ where g_m' and g_m'' are the first and second derivatives of the intrinsic transconductance, respectively.

$$IM3 = \frac{\left(\frac{3}{4}k_3A^3\right)^2}{2R_L} = \left(\frac{3}{4\sqrt{2}}\right)^2 \cdot \frac{k_3^2A^6}{R_L} = \left(\frac{3}{8\sqrt{2}}\right)^2 \frac{\left(g_m''\right)^2}{G_{ds}^2 \cdot R_L} \cdot A^6 \tag{2.8}$$

Using IP3 definition (linear part is equal to the third-order intermodulation distortion) to obtain A as shown in equation (2.9), the device IP3 can be obtained as equation (2.10).

$$k_1A = \frac{3}{4}k_3A^3 \tag{2.9}$$

$$IP3 = \frac{k_1^2A^2}{2R_L} = \frac{4}{3}\frac{g_m{}^3}{g_m{}'' \cdot G_{ds}^2 \cdot R_L} \tag{2.10}$$

In the linear equivalent circuit, a drain-source current model can be used for IM3 and IP3 estimated as equation (2.11) [6, 7].

$$i_{ds}\left(v_{gs}, v_{ds}\right) = \frac{\partial I_{DS}}{\partial V_{GS}} \cdot v_{gs} + \frac{\partial I_{DS}}{\partial V_{DS}} \cdot v_{ds} \tag{2.11}$$

Where v_{gs} and v_{ds} are the incremental gate and drain voltages, respectively. i_{ds} is linear terms of drain to source current. The nonlinear drain to source current is controlled by two voltages as shown in equation (2.12).

$$\begin{aligned} I_{DS}\left(V_{GS}, V_{DS}\right) = {} & a_0 + a_1V_{GS} + a_2V_{GS}^2 + a_3V_{GS}^3 + a_4V_{GS}^4 + a_5V_{GS}^5 + \ldots \\ & + b_0 + b_1V_{DS} + b_2V_{DS}^2 + b_3V_{DS}^3 + b_4V_{DS}^4 + b_5V_{DS}^5 \end{aligned} \tag{2.12}$$

The small-signal drain to source current can be modeled by means of a pair of separate elements Gm and conductance (Gds) shown in equation (2.13) and (2.14).

$$G_m\left(V_{GS}\right) = \frac{\partial I_{DS}\left(V_{GS}, V_{DS}\right)}{\partial V_{GS}} = a_1 + 2a_2V_{GS} + 3a_3V_{GS}^2 + 4a_4V_{GS}^3 + 5a_5V_{GS}^4 + .. \tag{2.13}$$

$$G_{ds}\left(V_{DS}\right) = \frac{\partial I_{DS}\left(V_{GS}, V_{DS}\right)}{\partial V_{DS}} = b_1 + 2b_2V_{DS} + 3b_3V_{DS}^2 + 4b_4V_{DS}^3 + 5b_5V_{DS}^4 + .. \tag{2.14}$$

Hence, the relationship between IM3, IP3 and Gm, Gds are shown in equation (2.15) and (2.16).

$$IM3 \propto \frac{\left(G_m''\right)^2}{G_{ds}^2 \cdot R_L} \cdot A^6 \tag{2.15}$$

$$IP3 \propto \frac{\left(G_m\right)^3}{G_m'' \cdot G_{ds}^2 \cdot R_L} \tag{2.16}$$

As a result, the IM3 is direct proportion to the second derivatives of the extrinsic transconductance (Gm″). The IP3 is an inverse proportion to Gm″ and direct proportion to third power of Gm. For this reason, the lower IM3 can be achieved by improving the Gm distribution flatness across the gate bias region. Meanwhile, higher Gm with flat Gm distribution also will result in higher IP3. In this paper, the extra doping either in the Schottky layer or in the channel layer was used to modify the drain-source current (I_{DS}) profile and to improve the Gm distribution flatness to improve device linearity.

2.3 Polynomial curve fitting technique

To further investigate the linearity performance of the three devices, polynomial curve fitting technique was applied on the transfer characteristic functions of these devices. The equation (2.12) was changed to I_{DS}-V_{GS} curves that were expressed in terms of a high order polynomial as equation (2.17):

$$I_{DS}\left(V_{GS}\right) = A_0 + a_1 V_{GS} + a_2 {V_{GS}}^2 + a_3 {V_{GS}}^3 + a_4 {V_{GS}}^4 + a_5 {V_{GS}}^5 + ... \tag{2.17}$$

Moreover, the IM3 levels incurred by the device can then be readily derived as [8, 9]:

$$IM3 = \frac{3}{8} a_3 A^3 + \frac{50}{32} a_5 A^5 \tag{2.18}$$

For a device with good linearity, I_{DS} should increase linearly with V_{GS}, therefore, a_1 should be larger and the higher order constants a_3 and a_5 should be minimized [9].

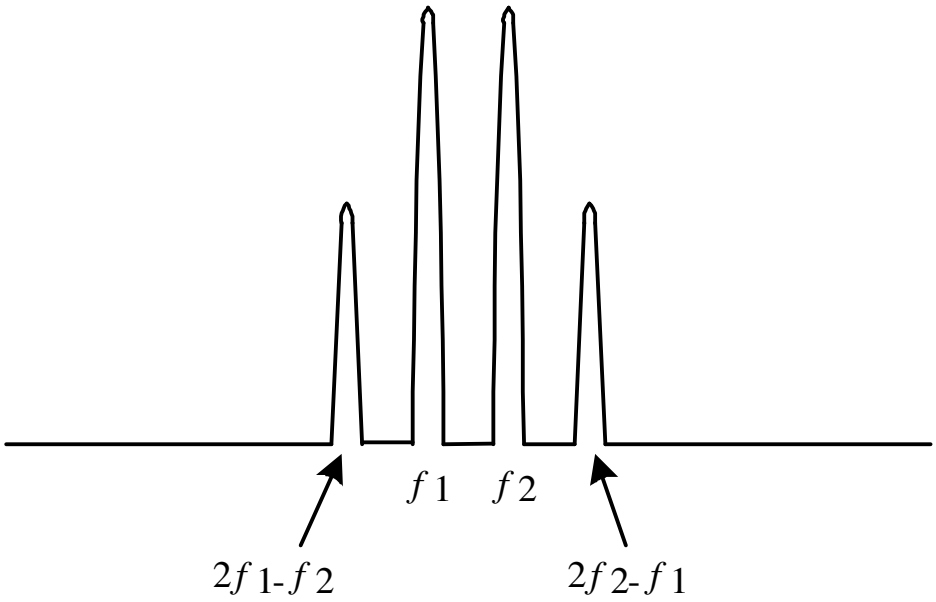

Figure 2-1 Output power spectrum of the two-tone input signal.

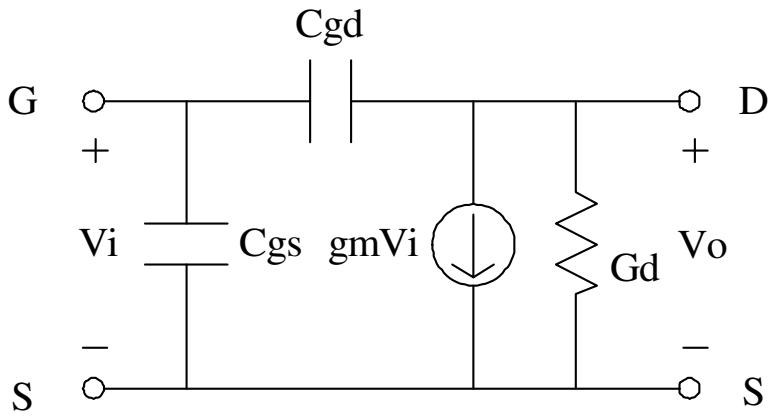

Figure 2-2 A simple equivalent circuit of PHEMT for linearity analysis.

Chapter 3

Fabrication of High Electron Mobility Transistors

3.1 Introduction of HEMT process

The HEMT process includes five major steps. They are: device active region definition, Ohmic metal deposition and annealing, gate formation by wet chemical recess and electron beam (EB) lithography, device passivation and air-bridge formation.

Device active region definition is to restrict the electrically conductive part of the wafer to specific parts of its surface area so that electrical current is restricted from flowing to other active areas. The electrically conductive portion is also called the "active region" of the wafer. The purposes of the active region definition include the active region formation, device isolation, reduction of parasitic capacitance, parasitic resistance, leakage current, and back-gating effect. It provides sufficient insulating area for device.

The device Ohmic contact is formed by Ohmic metal deposition and annealing. An Ohmic contact is a low resistance junction formed between metal and semiconductor interface. Lower contact resistance will result in lower device noise and lower power consumption for the device. Therefore, a heavily doped region was used near the metal-semiconductor interface to obtain a low resistance Ohmic contact.

The gate process include wet chemical recess and electron beam (EB) lithography. The size and position of the gate is critical to HEMT performance for high frequency operation. Therefore, most power HEMTs use a recessed gate geometry in which the gate stripe is placed in an etched slot for the device performance improvement. The gate recess process has two advantages. One is the gate is placed below the surface depletion layer of the surrounding material,

preventing surface depletion from restricting current under forward gate bias, and the other one is gate recess will reduce channel thickness and source-to-drain saturation current. Consequently, it can be used to increase device breakdown voltage, and decreased source-to-gate and gate-to-drain parasitic resistances. Because GaAs HEMTs are very sensitive to surface states in the gate area, therefore, after device gate metal deposition and lift-off process, a PECVD silicon nitride film was deposited to protect the devices from environmental contamination and mechanical damages.

Finally, plated air-bridges were used for the GaAs device interconnects. The air-bridge structure provides several advantages: these are lower parasitic capacitance, immunity to edge profile problems and the ability to carry substantial current. The fabrication process flow of the HEMT is shown in Fig.3-1. Low noise MHEMT and InGaP/InGaAs PHEMT with different structure and doping profiles were fabricated to investigate the device linearity improvement due to structure variation in this thesis. The detailed fabrication process of the MHEMT and InGaP/InGaAs PHEMT devices will be described in the following section.

3.2 MHEMT process

3.2.1 Device active region definition

Semi-insulating GaAs substrates have better electrical isolation than silicon substrate. “Mesa isolation” is the simplest way of providing isolation between devices and can be achieved by wet chemical etching. In the MHEMT devices fabrication, the wafer was etched to buffer layer to get a good isolation. We defined the device active region by photolithography. Then the wafer was mesa etched by a $H_3PO_4/H_2O_2/H_2O$ (5:1:40) solution. A mesa-sidewall etching was used to isolate the gate-leakage path [10] in this study. After mesa etching, we measured the etching depth by α-stepper to ensure the etch depth is sufficient, and checked the etched profile by scanning

electron microscope (SEM).

3.2.2 Ohmic contact formation

We use Au/Ge/Ni/Au as the ohmic metal with total thickness of 4100Å in the Ohmic contact formation of our MHEMT process. The Au/Ge alloy is the most commonly used because it forms low contact resistance ohmic and has good reliability. For the Ohmic metal layer determine, the germanium (Ge) is used for doping the GaAs and the nickel (Ni) is act as a wetting agent and prevents the AuGe metal from "balling up" during alloy.

For the Ohmic contact formation, first, the ohmic contact was defined by deep UV photolithography with undercut profile. Then O_2 plasma descum was used to remove the residual photo-resist on the open windows. We also dip samples in 10% HCl solution for 1 minute to remove oxide from the surface before depositing the ohmic metal. Finally, e-gun evaporation system was used to deposit Au/Ge/Ni/Au metal. The ACE was used for device lift-off procedure, then the wafer was thermally alloyed by using rapid thermal anneal system (RTA) at 310℃ for 30 seconds.

3.2.3 Recess and gate formation

Because dry etching will generate ion-bombardment damage on the surface and affect the device performance, in here, the wet chemical etching process was used for the device gate recess. In order to further increase gate-to-drain breakdown voltage, the double gate recess also was processed. The 1st recess slot was defined by e-beam photolithography to form the photo-resist layer. Then, a succinic acid/H_2O_2/H_2O solution was used to etch the cap layer and InAlAs Shottky layer until it reaches the target current. The target current is a critical parameter in HEMTs performance. So we measure the drain-to-source current during the recess process to control the target

current by curve tracer.

After removing the 1st recess photo-resist, the gate openings were defined by e-beam lithography to form the dual photo-resist layers with T-shaped profile. Then the succinic acid/H_2O_2/H_2O solution also was used to execute the 2nd recess. The 2nd recess can further increase the breakdown voltage.

Before the gate metal deposition, the sample was dipped in the 20% HCl solution for 15 seconds to remove the native oxide from the surface. And that gate metal was deposited by e-gun evaporation system. The gate metal used is Ti/Pt/Au=1000/1000/3000Å. Titanium provides good adhesion to substrate, platinum provides a barrier to prevent gold diffusing into GaAs, and gold provides high electrical conductivity. Finally the wafer was immersed into ACE to lift-off the undesired metal.

As a result, T-shaped gate has a large cross-section area at the top of the gate, and a short gate length in contact with the wafer. T-shaped gate (Fig.3-2) can reduce the gate resistance and capacitance. As the gate length is reduced, the gate resistance will obviously increase because of the reduction of gate cross-section area.

To fabricate the T-shaped gate, the dual photo-resist layers had been used. They consists of poly methyl methacrylate (PMMA) as the bottom layer, and copolymer P(MMA-MAA) as the top layer. Because of the sensitivity of copolymer is higher than that of PMMA, we can get a T-shaped profile.

3.2.4 Device passivation

For device passovation, the silicon nitride film was formed by PECVD. Silicon nitride is less permeable to ions than silicon dioxide, and therefore makes it the superior encapsulant. The wafer was first dipped in the solution of NH_4OH:H_2O=1:50 for 10 seconds to clean the surface and decrease the surface dangling bonds. The

silicon nitride film was grown at 250℃. RF power was 35W, and the precursors were SiH_4/Ar, NH_3, and N_2. The film thickness was about 1000Å and its refractive index was about 2.0, which were measured by ellipsometer.

The thickness of the silicon nitride film represents a trade-off between conflicting requirements. If the nitride film is too thin, the number of pinholes will be large and has less mechanical strength. If the nitride film is too thick, the parasitic capacitance will increase.

After the passivation process, the contact via was defined for interconnections. Then the silicon nitride film was etched by reactive ion etching (RIE) system. The reactive plasmas are CF_4 and O_2, the RF power is 80W, and the pressure is 60 mtorr.

3.2.5 Air-bridge plating

The major steps of air-bridge formation are shown in Fig.3-3. The plated metal on the GaAs devices is usually gold. Gold has many superior properties as compared to other metals. Gold plated interconnect, which has high electrical conductivity, is easily soldered or welded, and is resistant to oxidation and most acids, and is ductile. But gold has poor adhesion on the wafer surface, we have to deposit thin titanium layer firstly to improve the adhesion. The detailed air-bridge process flow is described as following.

First, a layer of photo-resist was spun and patterned to open areas over metal pads. Then, a thin coating of Ti/Au/Ti=300/500/300Å was applied to the entire wafer. The thin metal layer can conduct the plating current to the whole wafer. Next, a second coating of photo-resist was applied and patterned. Then the wafer was electroplated with gold for 2 μm thickness. After plating, the top resist layer, thin Ti/Au/Ti metal, and lower resist layer were removed individually, leaving only the plated airbridge.

After the air-bridge plating, the front-side process of MHEMT is completed, and the RF characteristics of the devices can be measured. The image of the finished 0.25x160- μm^2 device is shown in Fig. 3-4. It use multi-finger type and has a drain to source spacing of 2 μ m.

3.3 InGaP PHEMT process

The InGaP PHEMT process is similar to MHEMT process. There are five major process steps for the InGaP/InGaAs PHEMT fabrication. These include device active region definition, ohmic metal deposition and annealing, wet chemical recess, gate formation by electron beam (EB) lithography and lift-off process, device passivation and gold plating of the airbridges for the interconnects. The mesa etch was achieved by using HCl/H_2O (1:1) solution etching for the InGaP layer [11] and $HF/H_2O_2/H_2O$ (2:3:10) solution for other layers. The ohmic contacts were formed by AuGe/Ni/Au evaporation and were annealed at 355^0C for 30 seconds by rapid thermal annealing. Double recess was used for superior device linearity [12]. The gate recess was performed using a highly selective citric acid/H_2O_2/H_2O solution [3] to selectively remove the cap GaAs material and HCl/H_2O solution was used for the etching of the InGaP Schottky layer. The Ti/Pt/Au was then deposited as the Schottky gate by lift-off technique. The gate length and the source to drain spacing of the devices fabricated also were 0.25 μ m and 2 μ m respectively.

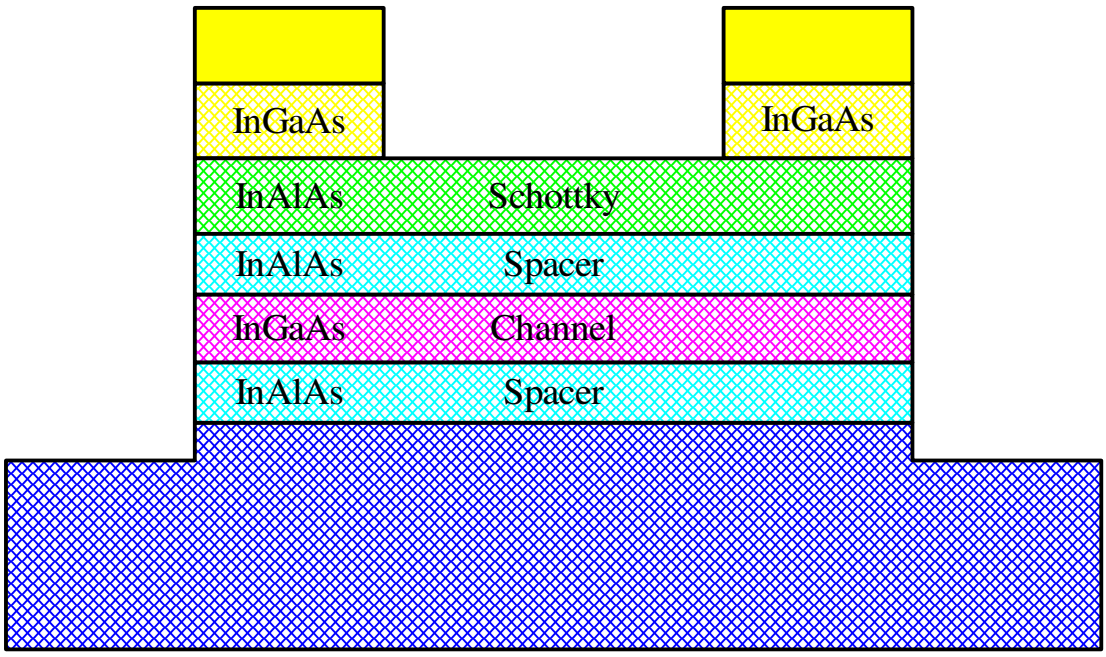

(a)

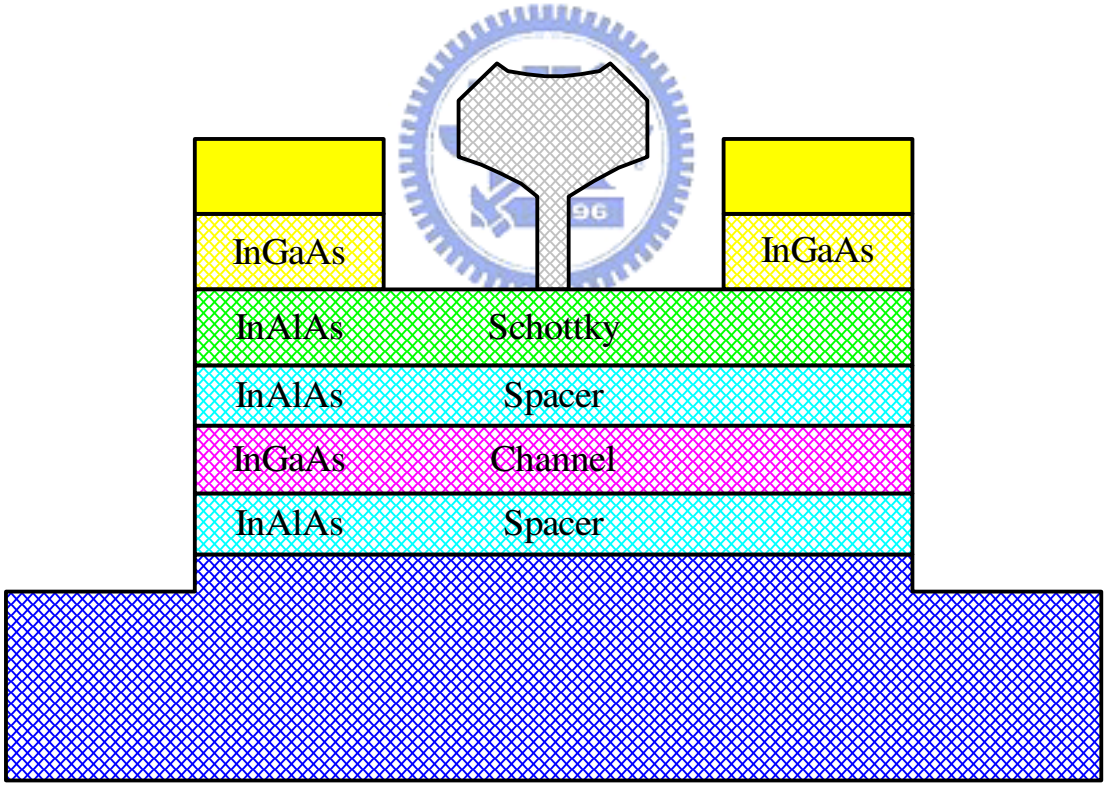

(b)

Figure 3-1 Process flow of the InGaP PHEMT: (a)Mesa isolation and ohmic contact formation, and (b) gate recess and gate formation.

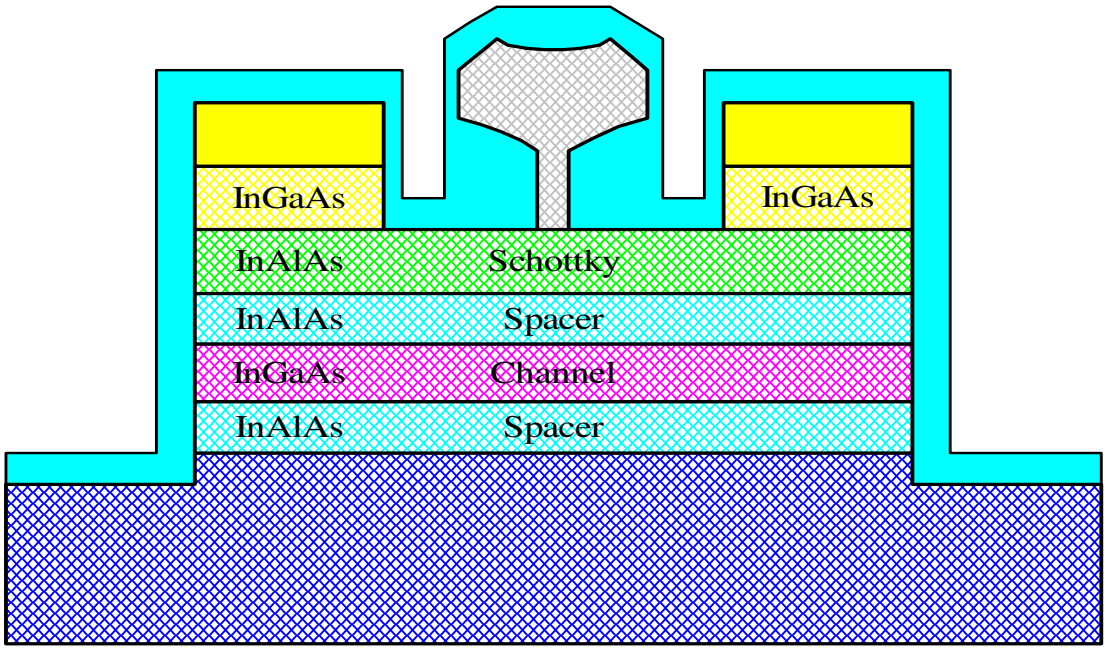

(c)

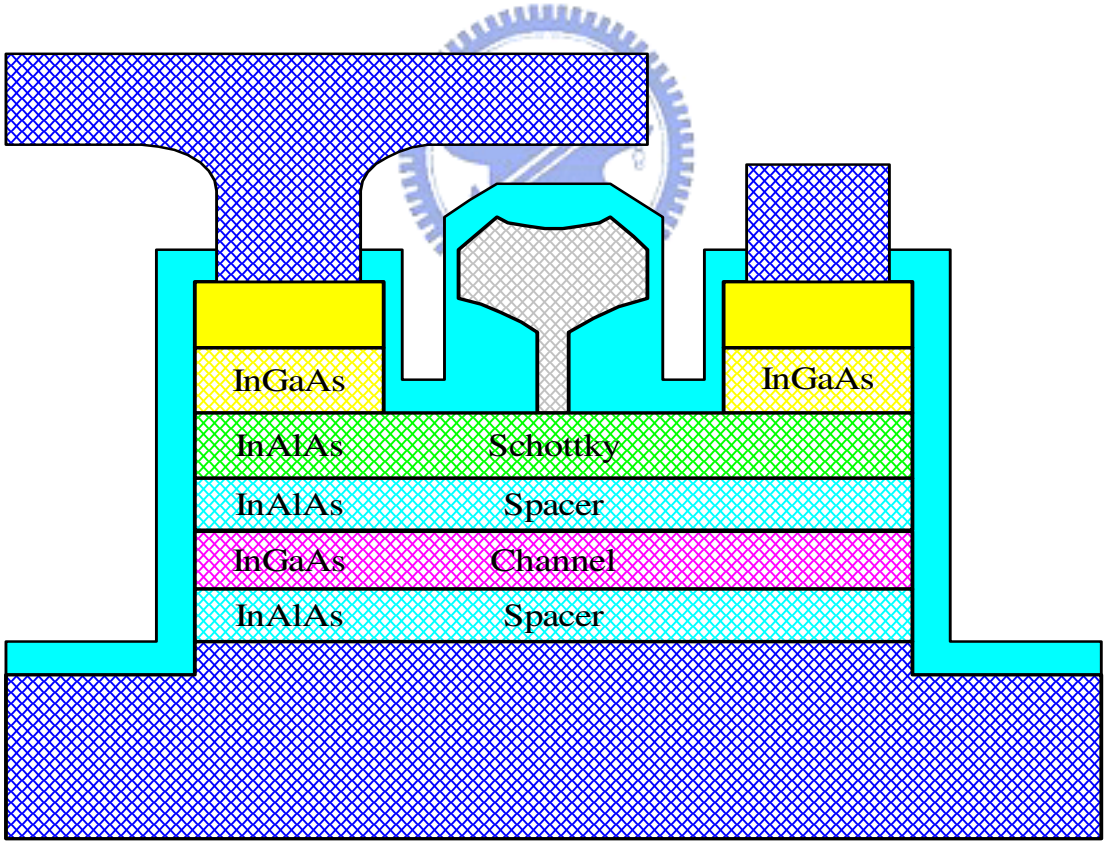

(d)

Figure3-1 Process flow of the HEMT. (c) Device passivation and contact via formation, and (d) air-bridge plating.

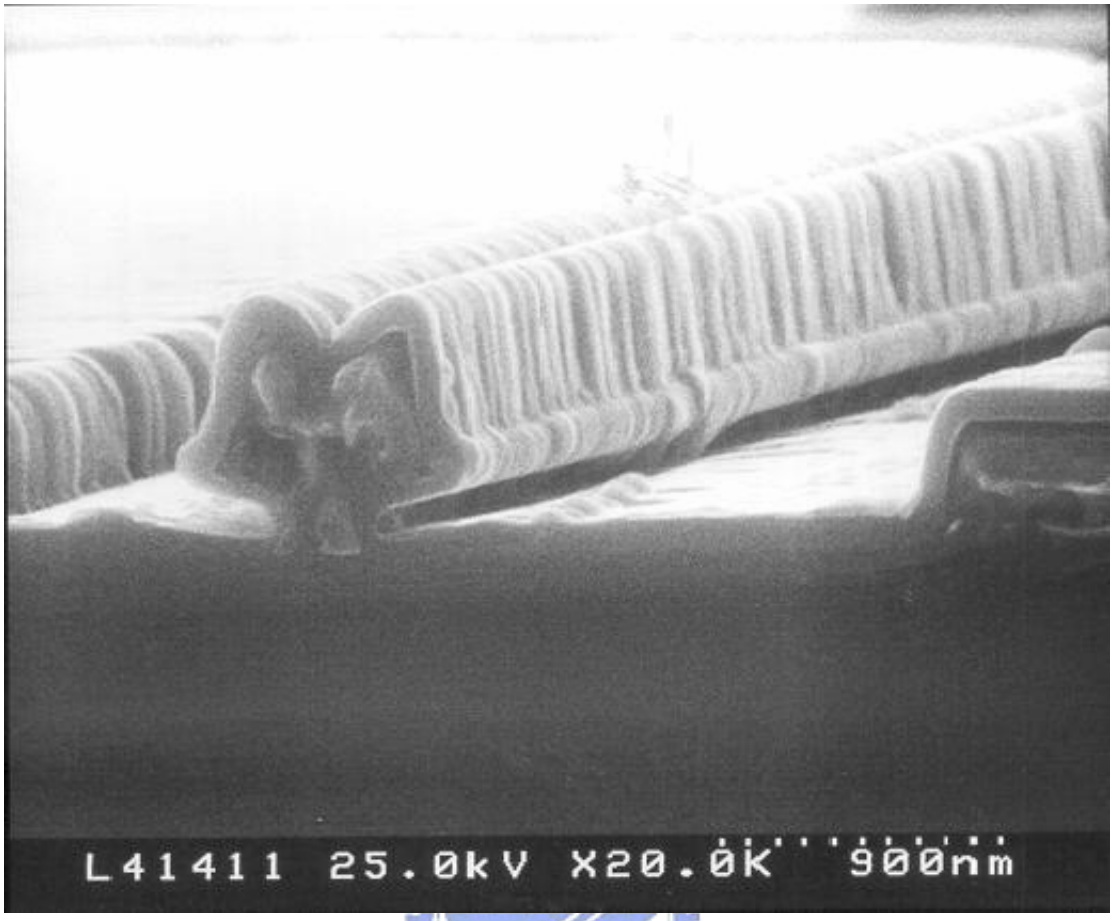

Figure 3-2 The SEM image of the T-shaped gate.

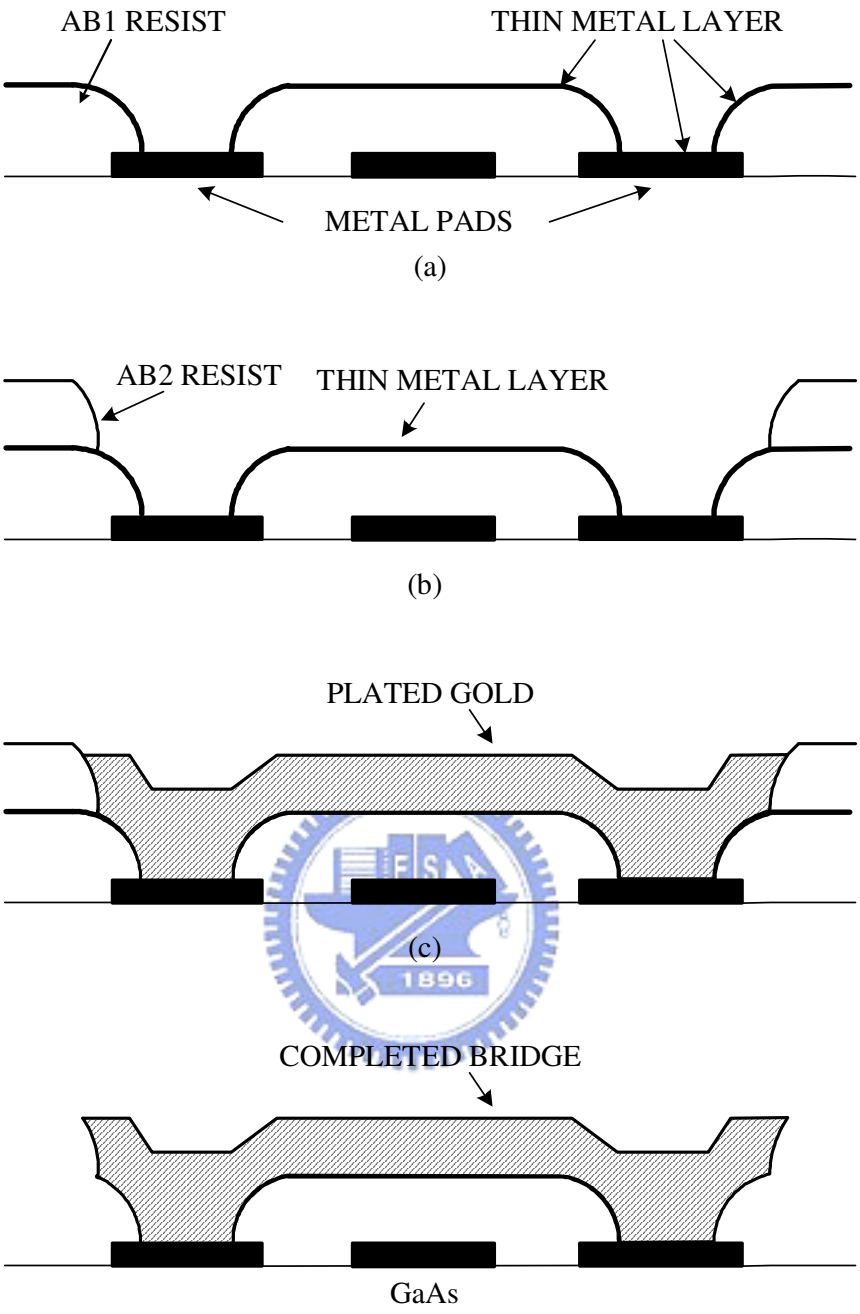

Figure 3-3 The major steps of air-bridge formation.

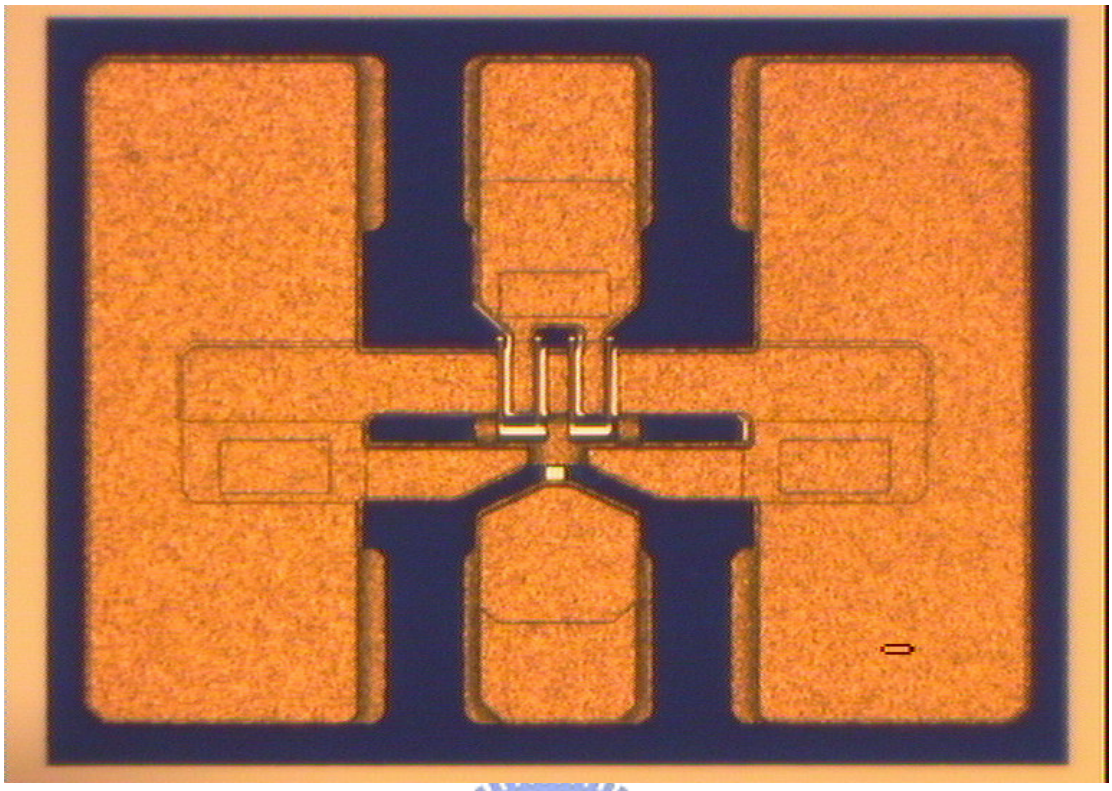

Figure 3-4 The Image of the finished 0.25x160 μ m^2 HEMT device

Chapter 4

A Low Noise Composite-Channel Metamorphic HEMT for Wireless Communication Applications

4.1 Introduction

InP high-electron-mobility transistors (HEMTs) with their superior carrier transport and carrier confinement characteristics the device of choice for high frequency applications. The high indium content of the channel (53%), which is lattice matched to the substrate is the primary factor behind the superior performance of HEMTs. However, the commercialization of this technology has been constrained by the small wafer size, fragility and a low volume of InP substrates resulting in high-cost monolithic microwave integrated circuits (MMICs) with low fabrication yields. Metamorphic high-electron-mobility transistors (MHEMTs) allows a wide range of Indium composition (from 30% to 80% based on the applications) in the InGaAs channel on a compositionally graded buffer, offering a low cost and manufacturabe alternative to InP HEMTs for low-noise, high power and reliable MMICs.

The performance of the conventional MHEMTs can be further refined with a band-engineered composite channel. A composite-channel MHEMT with an InAlAs graded buffer was grown by molecular Beam Epitaxy (MBE) on a 3-inch-diameter GaAs substrate. The device structure is shown in Fig.4-1(a). It contains an $In_{0.52}Ga_{0.48}As$ cap layer with a doping concentration of 3×10^{18} cm^{-3}, to achieve good ohmic contact. The InAlAs layer was used as the Schottky layer. Two δ-doped layers above and below the InAlAs spacer layers were used to increase the current density of the device. The composite-channel includes a top $In_{0.55}Ga_{0.45}As$ layer, a middle $In_{0.67}Ga_{0.33}As$ layer, and a bottom $In_{0.55}Ga_{0.45}As$ layer. The design of this structure

takes advantages of both the high drift velocity and low impact ionization of $In_{0.55}Ga_{0.45}As$ under high electric fields, as well as the high electron mobility of $In_{0.67}Ga_{0.33}As$ under low electric fields. Furthermore, this structure also has the advantage of good electron confinement [13] when compared with conventional MHEMTs. For comparison, a conventional MHEMT with the structure as shown in Fig.4-1(b) was also fabricated. The structure of the conventional MHEMT is the same as that of the composite- channel MHEMTs except for the channel layers.

4.2 Device performance

The developed 0.25x160- μ m^2 composite-channel MHEMT shows drain to source saturation current of 520mA/mm as shown in Fig.4-2(a). The extrinsic transconductance of the device is 773mS/mm at V_{DS} = 1.5V as shown in Fig.4-2(b). The gate to drain breakdown voltage is higher than 18.8 V as shown in Fig.4-3 and the channel breakdown voltage is larger than 3 volt. Because the composite-channel MHEMT has a better electron confinement property than the conventional MHEMT, it results in a flatter transconductance across the transconductance vs applied gate voltage curve, as shown in Fig.4-4. The third-order distortion of the signal is approximately determined by the following equation (2.16) [5]:

$$IP3 \propto \frac{(G_m)^3}{G_m'' \cdot G_{ds}^2 \cdot R_L}$$

Therefore, when the transconductance remains constant across the operating range of gate bias, the third-order distortions will be greater. Compared with that of the conventional MHEMTs, the transconductance of the composite-channel MHEMT is flatter, as shown in Fig.4-4. Therefore, it has higher linearity and output third-order intercept point (IP3) at the same DC bias, as shown in Table.4-1. The noise of the device at 6GHz was 0.23dB with 15.06dB associated gain, and the noise figure at

12GHz was 0.48dB with 11.42dB associated gain as shown in Fig4-5. The maximum frequency of oscillation f_{max} and the current gain cut-off frequency f_t of the composite channel MHEMT were 290 GHz and 110 GHz, respectively.

The outstanding performance of the device demonstrates that the composite channel metamorphic HEMT has a great potential for low noise and high linearity application at high frequencies.

4.3 Conclusion

We have fabricated composite-channel MHEMT grown by Molecular Beam Epitaxy (MBE) on GaAs substrates with InAlAs graded buffer. The $0.25\times160\ \mu m^2$ device with the novel channel structure exhibits a maximum frequency of oscillation f_{max} of 290 GHz and a current gain cut-off frequency f_t of 110 GHz. The noise figure of the device at 6 GHz is 0.23dB and the associated gain was 15.06dB. The IP3 of the device at 6GHz is 18.67 dBm. The composite channel metamorphic HEMT shows great potential for high linearity and low noise application at high frequencies. Future work will be focused on achieving optimized source drain configurations, further band engineering improvement in composite channel, optimization for higher power output at superior transconductances.

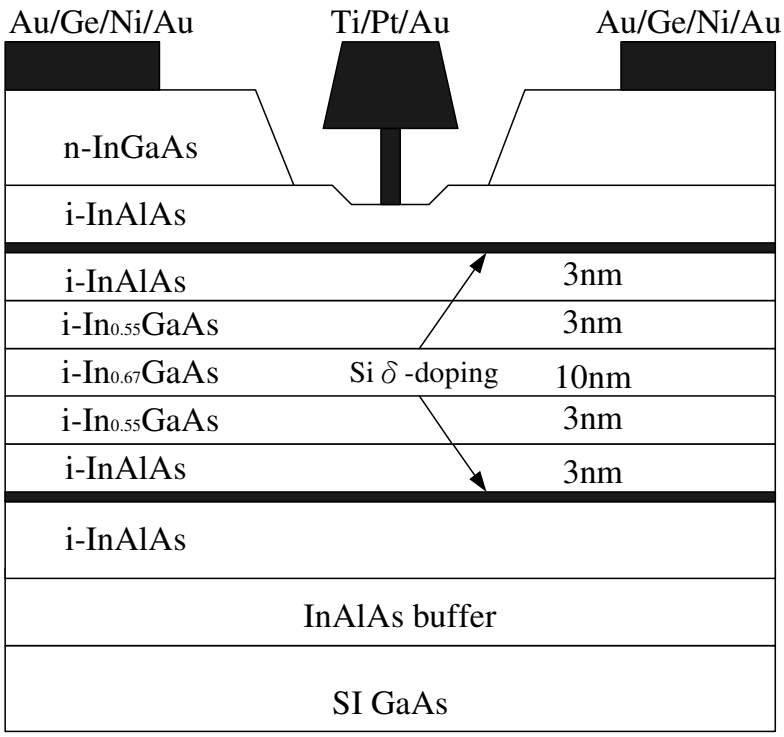

(a)

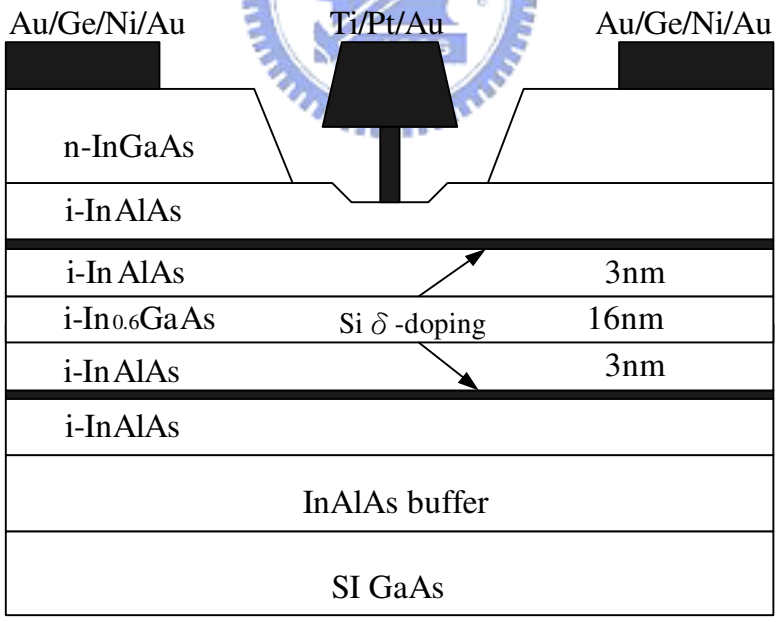

(b)

Figure 4-1(a) Structure of $In_{0.67}Ga_{0.33}As$ composite-channel MHEMT.

(b) Structure of $In_{0.6}Ga_{0.4}As$ conventional MHEMT.

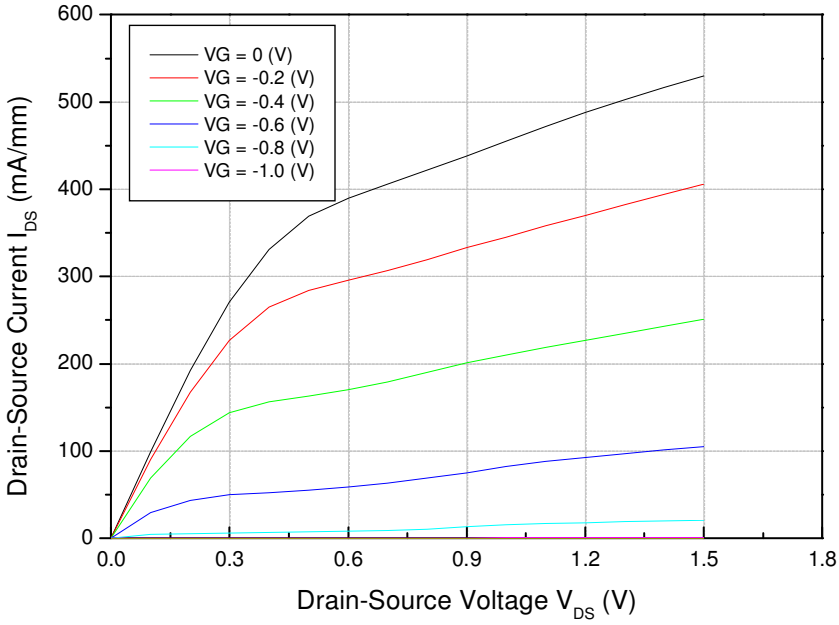

(a)

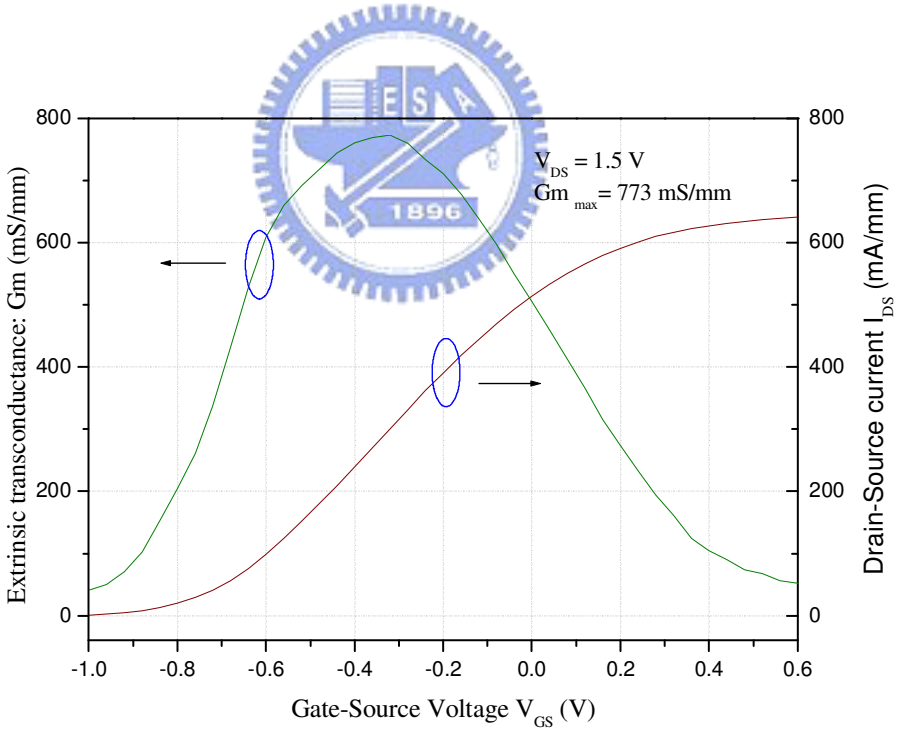

(b)

Figure4-2 (a) I-V characteristics (b) Extrinsic transconductances vs gate bias of the 0.25×160 μ m^2 $In_{0.67}Ga_{0.33}As$ composite-channel MHEMT.

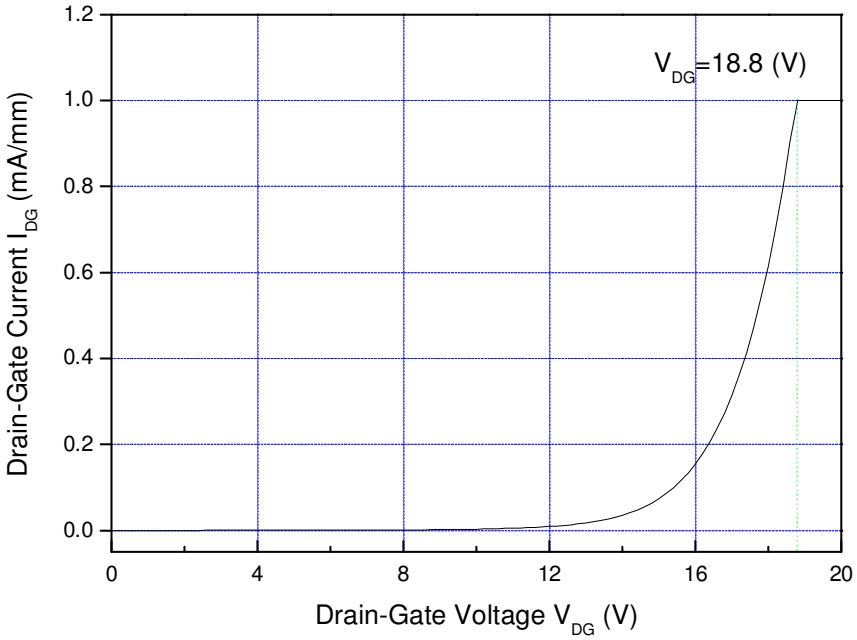

Figure 4-3 The gate to drain breakdown voltage of the 0.25×160 μ m^2 $In_{0.67}Ga_{0.33}As$ composite-channel MHEMT.

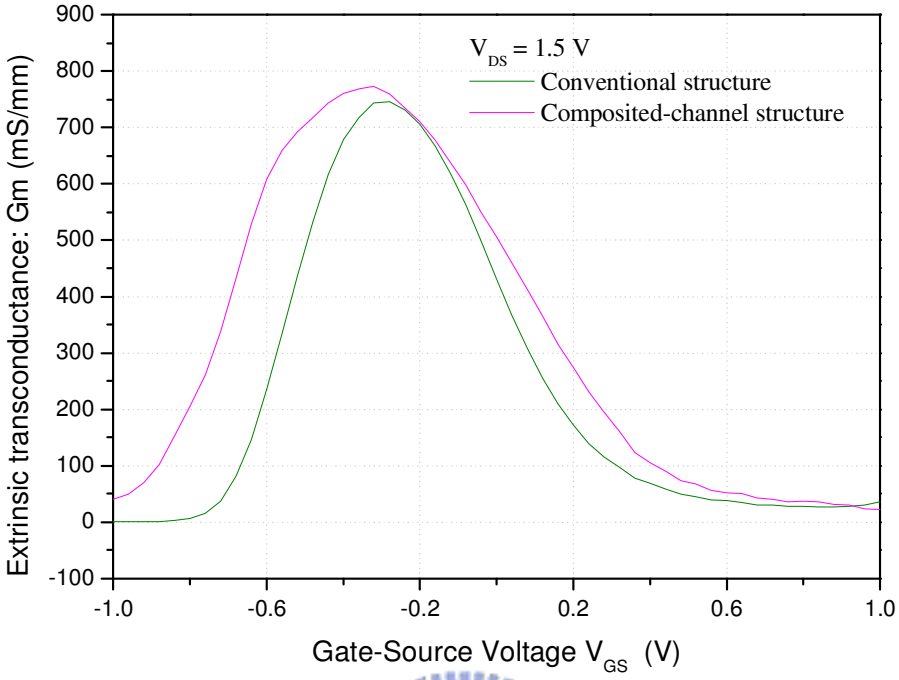

Figure 4-4 Extrinsic transconductances of the $In_{0.67}Ga_{0.33}As$ composite-channel MHEMT and the $In_{0.6}Ga_{0.4}As$ conventional MHEMT of the 0.25×160 μm^2 devices.

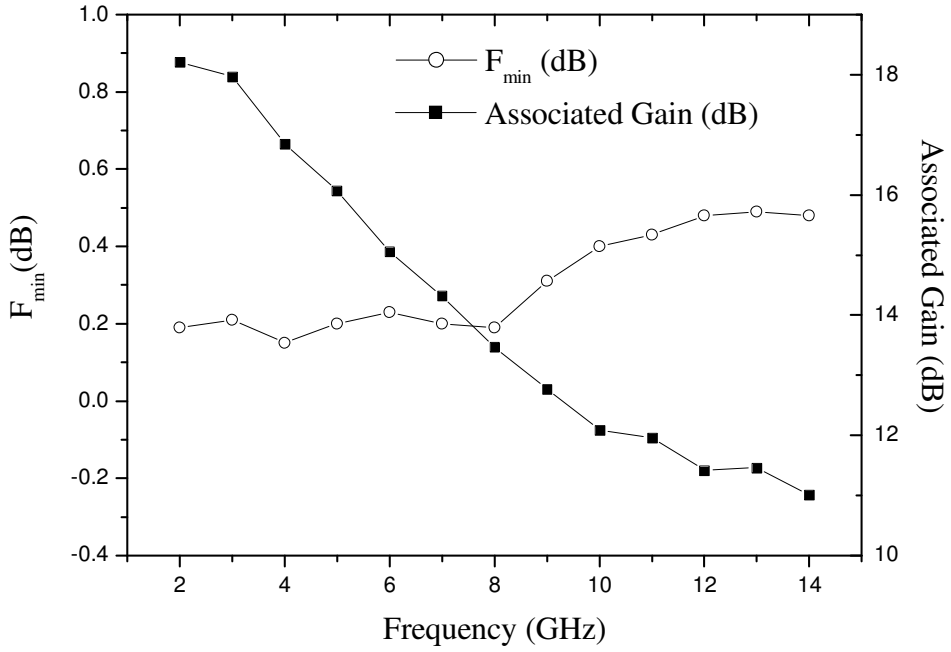

Figure 4-5. Noise and associated gain of the composite-channel MHEMT at V_{DS} = 1.5 V and I_{DS} = 50 mA/mm.

Table.4-1 Performance of the $In_{0.67}Ga_{0.33}As$ composite-channel MHEMT and the $In_{0.6}Ga_{0.4}As$ conventional MHEMT of the 0.25×160 μm^2 devices.

Device Type		Composite-channel Wg =160 μ m		Convention MHEMT Wg =160 μ m
Gm @ Vds=1.5V (mS/mm)		773		745.6
IP3 (frequency: 6GHz)	DC bias point: Vds=1.5V	Ids = 0.08 Idss	Ids = 0.17 Idss	Ids = 0.17 Idss
	P_{1dB}(dBm) 1dB compression output power	3.46	3.53	2.24
	IP3 (dBm)	18.67	16.75	14.07
	Δ(IP3-P_{1dB}) (dB)	15.21	13.22	11.83

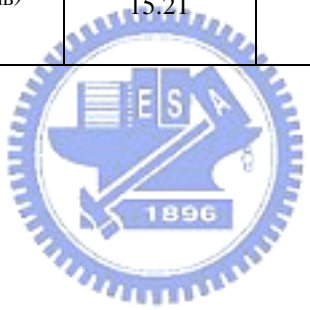

Chapter 5

Device Linearity Comparison of the Uniformly-Doped and the δ Doped $In_{0.52}Al_{0.48}As/In_{0.6}Ga_{0.4}As$ Metamorphic HEMTs

5.1 Introduction

For wireless communication applications, it is an important issue that the devices used in the system may produce nonlinear distortion and thus degrade the signal to noise ratio of the system. Consequently, the device structures need to be tailored to improve the RF performance of the system. Metamorphic high electron mobility transistors (MHEMT) have been widely investigated for low noise and high power applications in recently years [14-17]. The main advantage of MHEMT is that it uses high indium content $In_xGa_{1-x}As$ channel with In composition ranging from 30% to 80 % that results in higher electron mobility for the device. Therefore, MHEMT offers a low cost alternative to the high performance, but more expensive InP HEMTs.

Delta doping and uniformly doping are two typical doping types for HEMTs. The performances of HEMT with these two different types of dopings had been studied before [18, 19]. However, no paper on the linearity performance of these two kinds of HEMTs ever reported. The $In_{0.52}Al_{0.48}As/In_{0.6}Ga_{0.4}As$ MHEMTs with different doping profiles are studied in this paper for device linearity comparison. Fig.5-1 shows the two kinds of device structures studied, one with uniform-doping in the $In_{0.3}Al_{0.7}As$ layer and another one with δ doping between $In_{0.3}Al_{0.7}As$ and $In_{0.52}Al_{0.48}As$ layer. These wafers were grown by Molecular Beam Epitaxy Method (MBE) on 3-inch GaAs substrates with InAlAs graded metamorphic buffer. The $In_{0.52}Ga_{0.48}As$ layer was used as the cap layer with doping concentration of 3×10^{18} cm^{-3} to obtain good Ohmic contacts. The $In_{0.3}Al_{0.7}As$ Schottky layer has high etch selectivity with the $In_{0.52}Ga_{0.48}As$ cap layer, which provides excellent gate recess uniformity. Dual

channels with $In_{0.52}Al_{0.48}As$ spacer layers are designed to increase the current density, provide uniform electron distribution and improve the device linearity [17,18].

5-2 Results and discussion

The electrical characteristics of the two structures in Fig.5-1 were studied and analyzed. Fig.5-2 shows the drain to source current (I_{DS}) vs gate to source voltage (V_{GS}) curves of the $0.3\times160\ \mu m^2$ $In_{0.52}Al_{0.48}As/In_{0.6}Ga_{0.4}As$ MHEMT devices when biased at V_{DS} = 1.5V. The gate to drain breakdown voltages of the δ doped and the uniformly-doped device were 7.2V and 3.8V respectively. Compared to the δ doped device, the uniformly-doped device has lower I_{DSS} (I_{DS} @ V_{GS}=0) with more straight I_{DS} vs V_{GS} curve. Extrinsic transconductance (Gm) vs. gate to source voltage (V_{GS}) curves are shown in Fig.5-3. Even though the δ doped device has higher peak Gm, the Gm vs I_{DS} curve of the uniformly-doped device is flatter than the δ doped device. According to the device simulation results, the uniformly doped device has more uniform electron distribution in the quantum well region than the δ doped device. This explains why the uniformly doped device has flatter Gm vs I_{DS} curve. To investigate the linearity performance, the I_{DS}-V_{GS} curves were expressed in terms of a fifth order polynomial as equation (2.17):

$$I_{DS}(V_{GS}) = A_0 + a_1V_{GS} + a_2V_{GS}^{\ 2} + a_3V_{GS}^{\ 3} + a_4V_{GS}^{\ 4} + a_5V_{GS}^{\ 5} + \ldots.$$

The device linearity is related to the flatness of the derivative of Gm with V_{GS}, i.e., a_1 should be larger and a_3/a_1 and a_5/a_1 should be minimized. The coefficients of these two devices extracted from the measurement data are listed in Table5-1. The uniformly-doped MHEMT shows higher a_1, lower a_3/a_1 and a_5/a_1. Finally, IP3 of these devices were measured to investigate the effects of different types of doping on the device linearity. Because IP3 is a function of several parameters, for comparison,

we kept the V_{DS} at 1.5V, tuning maximum power with different I_{DS} bias for IP3 comparison. Fig.5-4 shows the device IP3 with different bias currents. For IP3 measurement, the load impedance was firstly tuned for maximum power for each individual device. Then the IMD3 (third-order inter-modulation distortion level) was measured and plotted as a function of input power under given DC bias conditions. IP3 was determined by the intercept point of the Pout and IMD3 curves (as functions of input power) after extrapolation. Two signals with the same amplitude but 1MHz apart in frequency at 6GHz were used as the input for IMD3 measurement. The uniformly-doped MHEMT has higher IP3 as compared to the δ doped device at a wide range of bias currents. The measured maximum IP3 of the uniformly-doped MHEMT was 19.83 dBm and that of the δ doped device was 16.98 dBm. Higher Δ (IP3-P1dB) of 13.66 dB was observed for the uniformly-doped MHEMT compared to the data of 12.1 dB observed for the δ doped one. In addition, the uniformly-doped MHEMT demonstrates a much higher IP3 to DC power consumption ratio ($IP3/P_{DC}$) of 6.21 as compared to the δ doped device of 1.96 (Table5-2).

5-3 Conclusion

The uniformly-doped and δ doped $In_{0.52}Al_{0.48}As/In_{0.6}Ga_{0.4}As$ MHEMTs were fabricated and the device linearity was compared. Even though the δ doped device has higher peak transconductance, the uniformly-doped MHEMT shows much better device linearity. This is because the uniform doped device has more uniform electron distribution in the quantum well region which enables the device to possess straight I_{DS} versus V_{GS} curve and more flat G_m versus I_{DS} curve, and in turn results in much higher IP3 levels, higher Δ and higher $IP3/P_{DC}$. Thus, the uniformly-doped MHEMT device is more suitable for the modern digital wireless communication systems which impose very stringent linearity requirement for the devices.

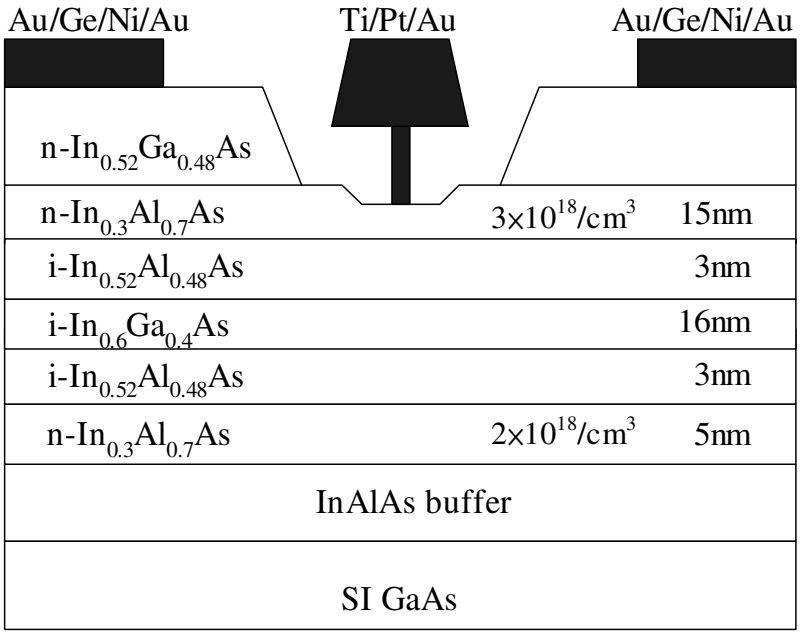

(a)

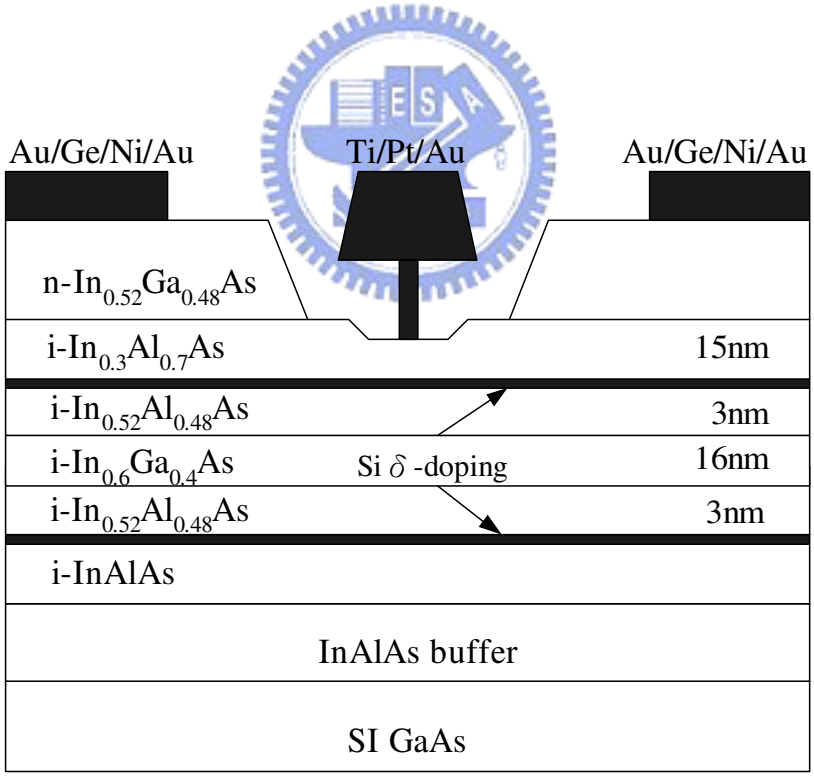

(b)

Figure 5-1 Structure of the $In_{0.52}Al_{0.48}As/In_{0.6}Ga_{0.4}As$ MHEMT: (a) Uniformly-doped, (b) δ doped.

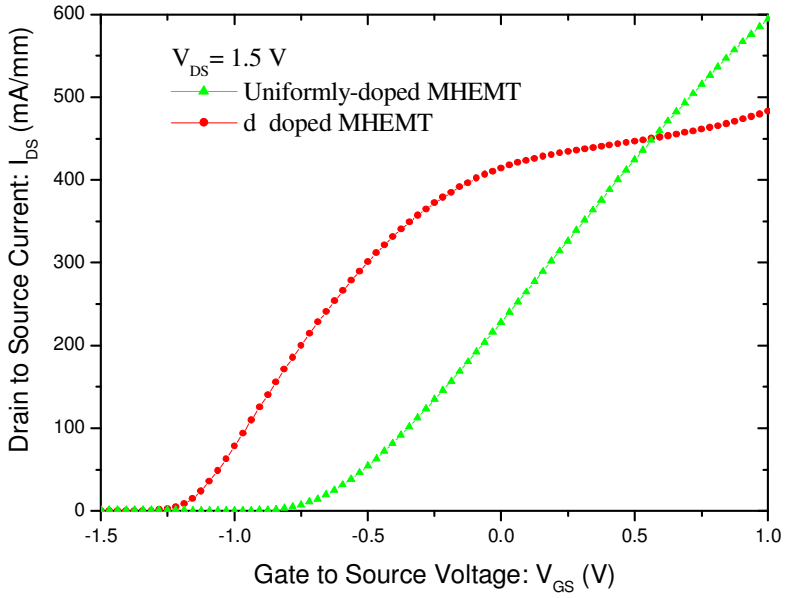

Figure 5-2 Drain to source current (I_{DS}) vs gate to source voltage (V_{GS}) of the 0.3× 160 μ m^2 $In_{0.52}Al_{0.48}As/In_{0.6}Ga_{0.4}As$ MHEMT devices.

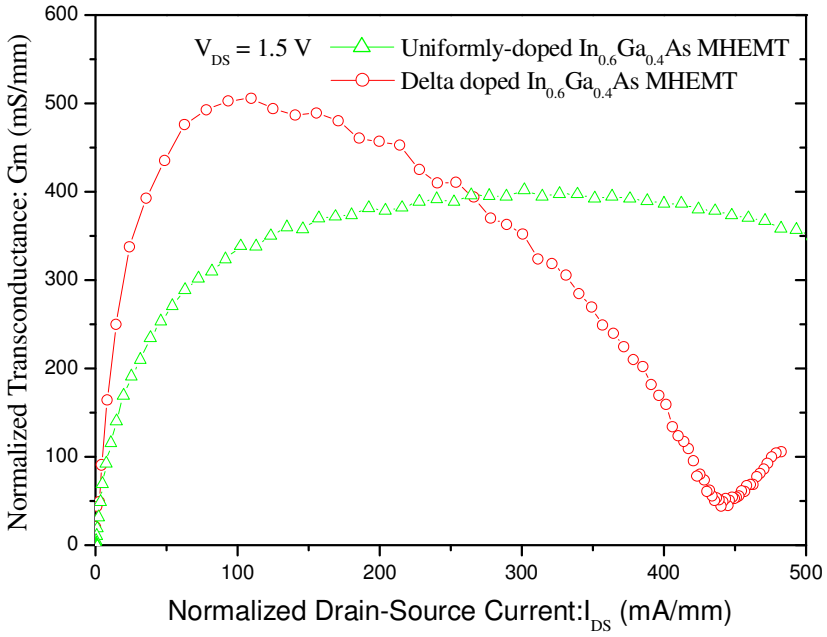

Figure 5-3 Extrinsic transconductance (G_m) vs drain to source current (I_{DS}) of the 0.3× 160 μ m^2 $In_{0.6}Ga_{0.4}As$ MHEMT devices.

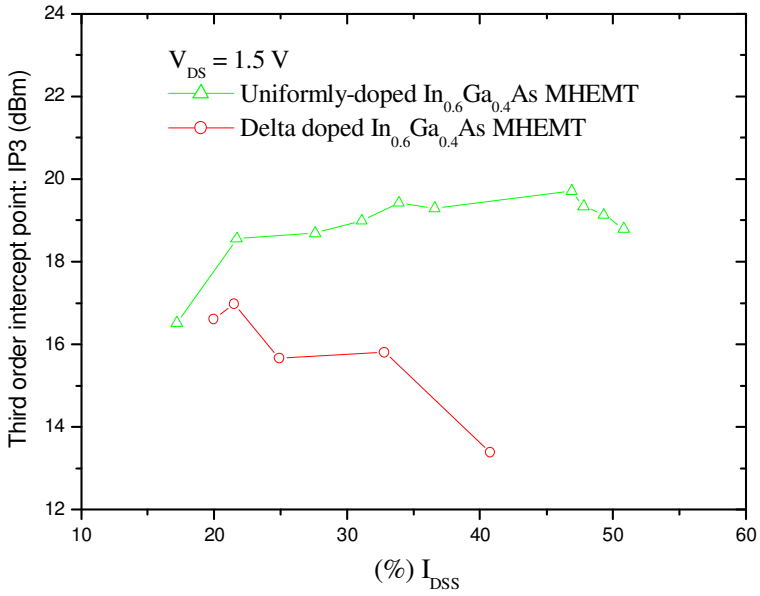

Figure 5-4. Comparison of device linearity of the uniformly-doped and the δ doped $In_{0.52}Al_{0.48}As/In_{0.6}Ga_{0.4}As$ MHEMTs.

Table5-1 Comparison of the DC characteristics of the Uniform-doped and the δ doped $In_{0.52}Al_{0.48}As/In_{0.6}Ga_{0.4}As$ MHEMTs.

Device Type	δ doped $In_{0.6}Ga_{0.4}As$ MHEMT	Uniformly-doped $In_{0.6}Ga_{0.4}As$ MHEMT
I_{DSS} (I_{DS} @ V_{GS}=0, mA/mm)	414.5	228.0
Gm_{max} (mS/mm)	506.0	401.4
Pinch off voltage:(V)	-1.17	-0.90
a_0	0.06634	0.03627
a_1	0.01835	0.06445
a_2/a_1	-1.555	0.131
a_3/a_1	1.215	-0.359
a_4/a_1	0.403	-0.045
a_5/a_1	-0.472	0.106

Table5-2 Comparison of the IM3 and IP3 of the Uniformly-doped and δ doped $In_{0.52}Al_{0.48}As/In_{0.6}Ga_{0.4}As$ MHEMTs.

Device Type	DC bias point: V_{DS} = 1.5V				
	I_{DS} (mA)	Operation frequency: 6GHz			
		P1dB (dBm)	IP3 (dBm)	Δ (IP3-P1dB) (dB)	$IP3/P_{DC}$
δ doped $In_{0.6}Ga_{0.4}As$ MHEMT	16.72	4.88	16.98	12.1	1.96
Uniformly-doped $In_{0.6}Ga_{0.4}As$ MHEMT	10.32	6.17	19.83	13.66	6.21

Chapter 6

A Low Noise InGaP PHEMT with AlGaAs spacer for High IP3 Application

6.1 Introduction

A low noise InGaP pseudomorphic high-electron-mobility transistors (PHEMTs) with AlGaAs spacer for high linearity application is developed. The device structure is as shown in Fig.6-1. It uses high doping concentration n^+-GaAs as cap layer to form good ohmic contact for the drain and source electrodes. The InGaP layer is used as the Schottky layer. The use of InGaP instead of AlGaAs as the Schottky layer for the PHEMT has the following advantages. Foremost, InGaP has higher energy band gap that can reduce the gate leakage current. Additionally, InGaP does not form deep-complex (DX) center at the desired doping level. Finally, high etch selectivity between InGaP and GaAs can be achieved, which improve the gate recess uniformity. In this study, we use AlGaAs as the spacer layer above and below InGaAs channel layer to increase the electron mobility, and high electron mobility of 6410 cm^2/Vs in the two dimensional electron gas (2DEG) channel region was achieved. This is believed to be highest electron mobility formed in the InGaP/AlGaAs/InGaAs PHEMT. Two delta-doped layers are used above and below the quantum well region to improve the transconductance flatness of the device [8,13]. Lastly, AlGaAs/GaAs superlattice was used to reduce the leakage current from the substrate.

6.2 Result and discussion

Due to the use of the InGaP Schottky layer and the AlGaAs spacer with dual delta doped structure, the device exhibits very low leakage current, low-noise with very high IP3 characteristics that is of great use for microwave applications.

The fabricated 0.25 × 160-μm^2 PHEMT device shows a saturation current of 243 mA/mm and the high extrinsic transconductance is 414.2mS/mm at V_{DS} = 1.5V as shown in Fig.6-2. The device drain to gate breakdown voltage can reach up to 15.2 V as shown in Fig.6-3. The 160 μm gate-width device has a noise figure of 0.59dB with 11.7dB associated gain at 12 GHz and the f_t and f_{max} are 80 GHz and 190 GHz respectively. The 0.25 × 300-μm^2 PHEMT device shows high output 3 order Intercept point (IP3) of 28.1dBm and the output power 1 dB compression (P_{1dB}) of 11.1dBm with Gain 16.2dB when DC bias at Vds = 2.4V, Ids = 28.6mA @ 6GHz as shown in Fig.6-4. Compared with the conventional AlGaAs/InGaAs PHEMT data, the InGaP/AlGaAs/InGaAs PHEMT developed has high Δ(IP3-P_{1dB}) and high IP3/P_{DC} ratio as shown in Table6-1[7]. Furthermore, gate leakage current of the device is very low. Fig.6-5 shows the gate current against reverse gate-source voltage with different drain-source bias, the gate current is 36 μA/mm at V_{DS} = 7V, V_{GS} = -0.8V.

6.3 Conclusions

An InGaP/AlGaAs/InGaAs PHEMT with very low noise figure, low third-order distortion, and low dc power consumption is developed. The outstanding performance of the device is attributed to the use of high band gap InGaP as the Schottky layer so as to improve the noise figure and reduce the gate leakage current, along with the use of AlGaAs as the spacer to improve the electron mobility, and the use of dual delta doped layers to improve the device linearity. The developed InGaP/AlGaAs/InGaAs PHEMT with very low noise figure and leakage current and very high IP3 is of great use for the wireless communication applications.

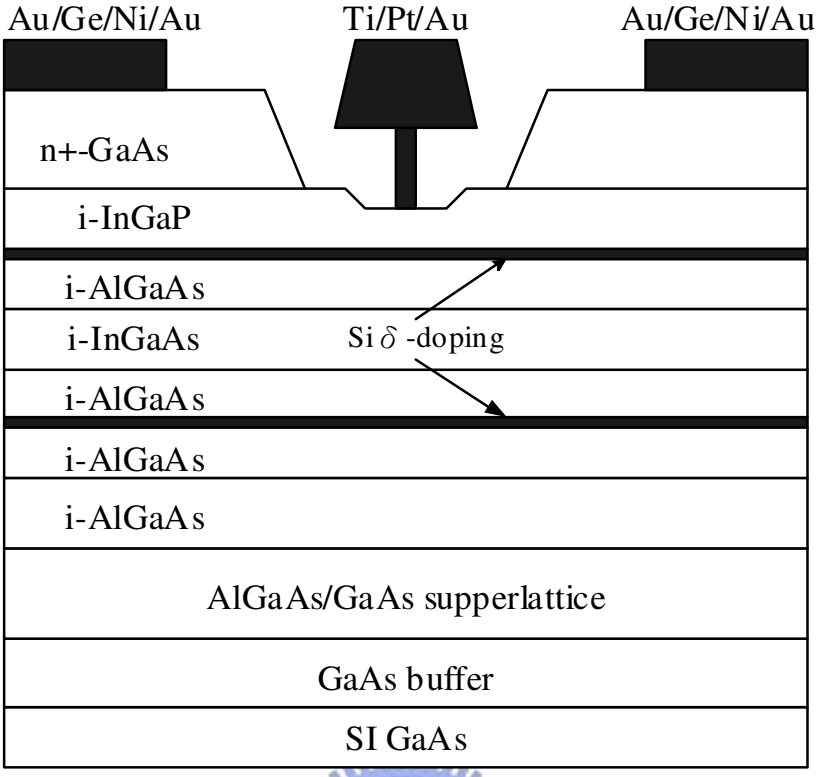

Figure6-1 Structure of InGaP/AlGaAs/InGaAs PHEMT.

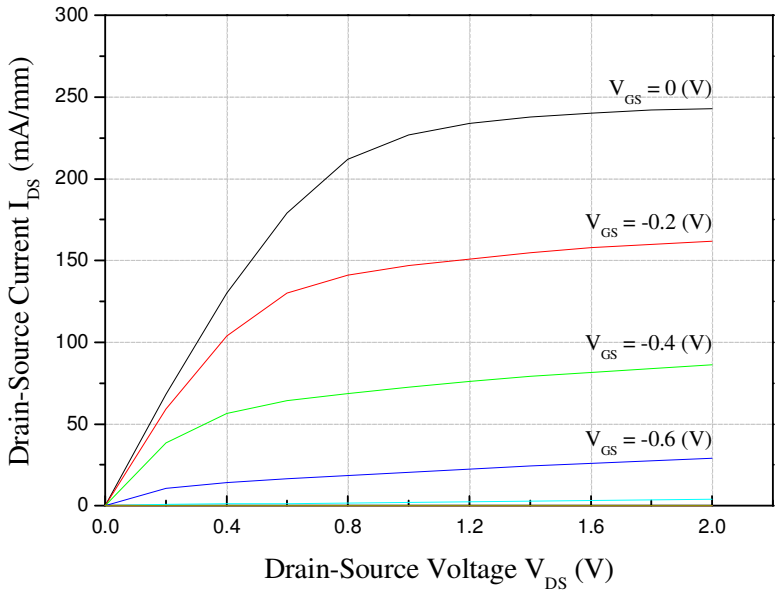

(a)

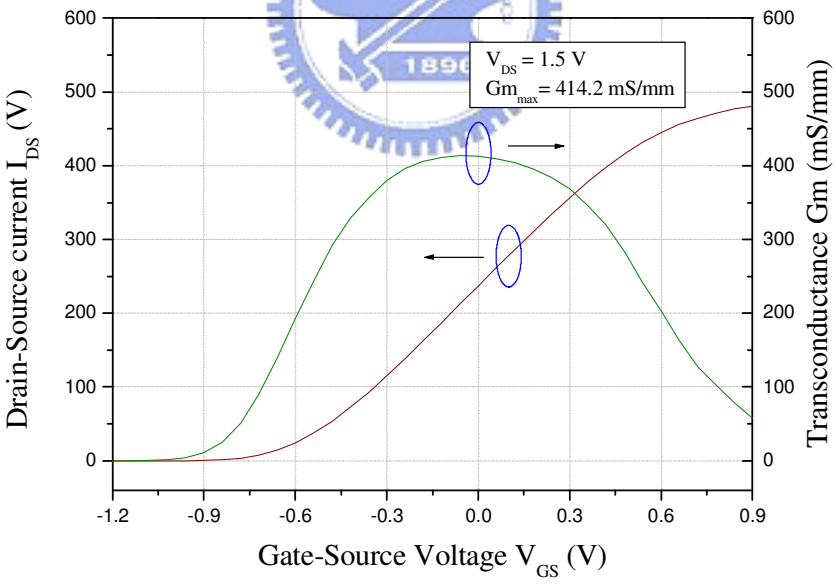

(b)

Figure6-2. The 0.25x160 μ m^2 InGaP/AlGaAs/InGaAs PHEMT DC characteristics:

(a) I-V characteristics, (b) Transconductance vs V_{GS} and I_{DS} curves.

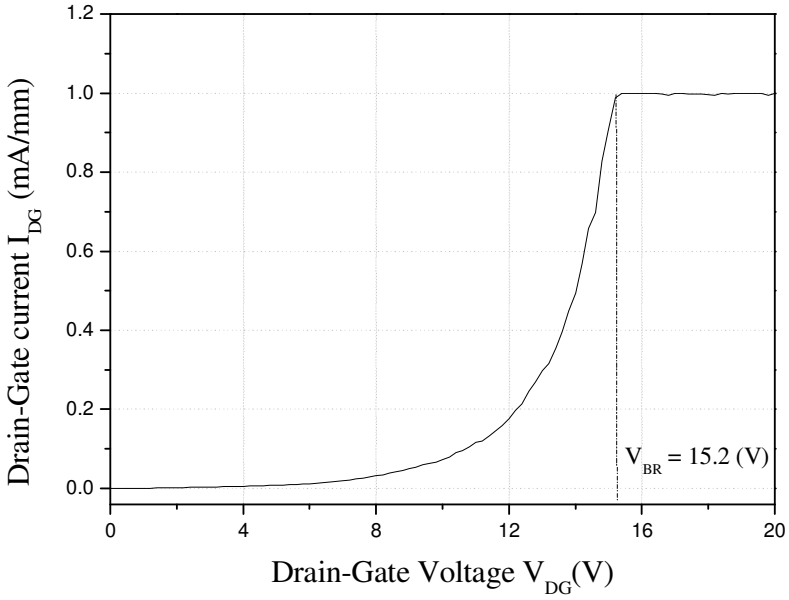

Figure6-3. The Drain to Gate breakdown voltage of the 0.25x160 μ m^2 InGaP/AlGaAs/InGaAs PHEMT.device

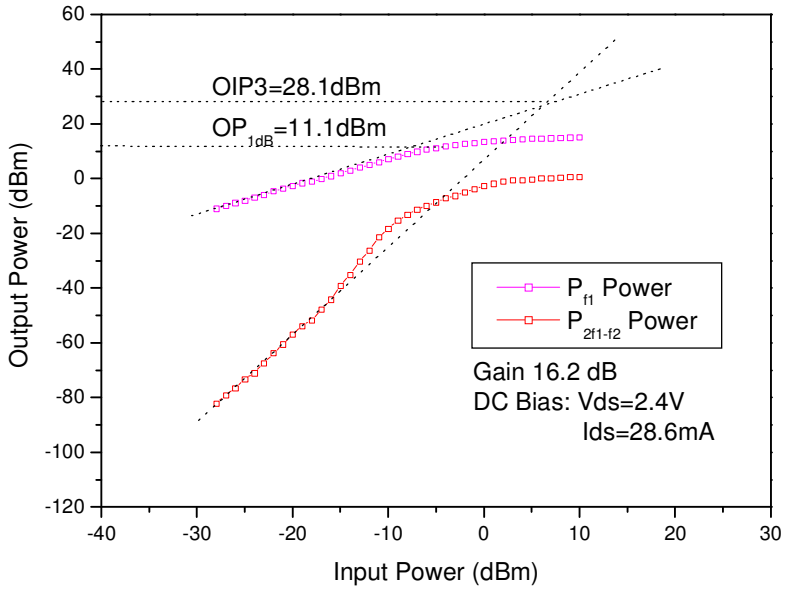

Figure6-4. Measured Third-Order Products and Fundamental Power of a 0.25x300 μ m^2 InGaP/AlGaAs/InGaAs PHEMT.

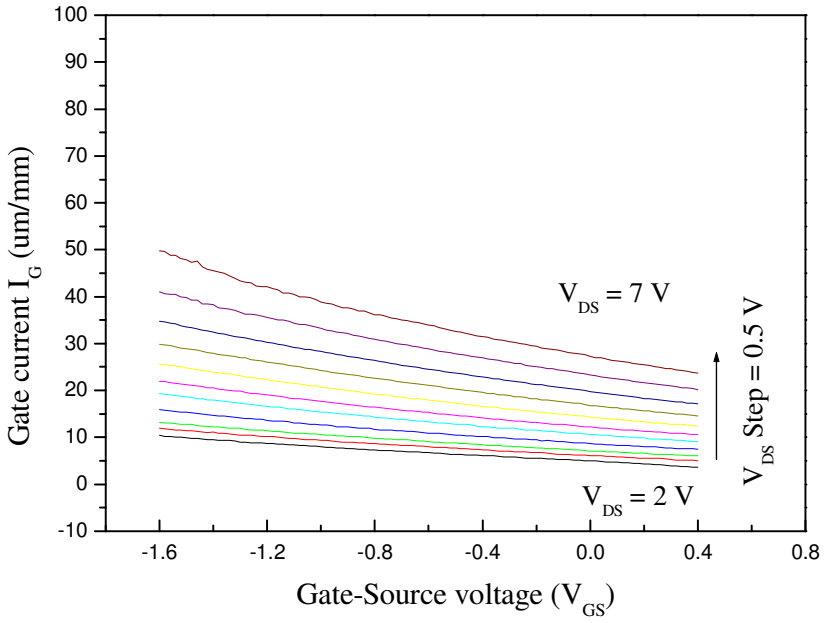

Figure6-5 InGaP/AlGaAs/InGaAs PHEMT Gate leakage current.

Table6-1 Comparison noise figure and IP3 with AlGaAs/InGaAs PHEMT.

Device Type	Gm (mS/mm)	Fmin(dB) at 6GHz Wg=160μm	IP3 with Wg = 300μm at 6GHz			
			1dB comp Pout(dBm)	IP3 (dBm)	Δ(IP3-P1dB) (dB)	IP3/P_{DC}
InGaP/AlGaAs/InGaAs Double delta-doped PHEMT	414.2	0.4	11.1	28.1	17.0	9.4
AlGaAs/InGaAs Double delta-doped PHEMT	432.0	0.6	12.7	23.0	10.3	1.6

Chapter 7

The δ Doped InGaP/InGaAs PHEMTs with Doping Profile Modification for Device Linearity Improvement

7.1 Introduction

Multi-channel transmission is a common practice used for signal transmission in modern wireless communication systems. When the operating frequencies of the system are more than two and the neighboring frequencies are located closely to each other, the device used in such system will generate intermodulation distortion. Among all the intermodulation distortions incurred by the devices, third-order intermodulation distortion (IM3) usually dominates and thus determines the linearity performance of the device. Therefore, IM3 has become the important figure of merit for the devices used for modern wireless communication applications.

InGaP/InGaAs PHEMT has been widely used in various high performance wireless communications systems [19, 20]. It was popular because the InGaP Schottky layer does not form deep-complex (DX) center at the desired doping level as the conventional AlGaAs layer does. High etch selectivity between InGaP and GaAs materials also results in better controllability for the device fabrication [21]. Consequently, in this paper, we study the δ doped InGaP/InGaAs pseudomorphic high-electron-mobility transistor (PHEMT) with extra-doping at the Schottky layer (Schottky layer doped) and the channel region (channel doped) for device linearity improvement through lowering the overall IM3 distortion level incurred by the device.

For linearity assessment, nonlinear transfer function based analysis method was used. Previously published results revealed that the variation of extrinsic transconductance (Gm) with respect to the gate bias plays an important role in the

IM3 levels. Hence, improving the flatness of the Gm profile will result in lower IM3 levels and higher third-order intercept point (IP3), and thus improve the device linearity [12]. The structure of the δ doped InGaP/InGaAs PHEMT is shown in Figure7-1. Two Si-planar-doped layers with doping concentration of 4 x 10^{12}/cm^2 and 2 x 10^{12}/cm^2 were used to supply high carrier concentration in the quantum well at the spacer and channel interface. For linearity improvement, the effects of light doping in the Schottky layer and in the channel layer were studied to improve the flatness of the Gm distribution under different gate bias conditions. The concentration of the extra doping in these layers was n = 5×$10^{17}$$cm^{-3}$. However, the extra doping will result in more impurity scattering and decrease of the carrier mobility as compared to the conventional δ doped device especially for the channel doped device [22]. Note that the electron mobility of the channel doped device in this study was 3500 cm^2/V.sec which was smaller than the Schottky layer doped device (4100 cm^2/V.sec) and the δ doped device (4200 cm^2/V.sec) due to the impurity scattering in the channel.

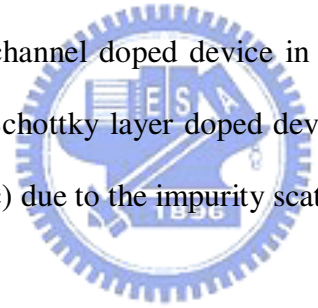

7.2 Device structure

According to the device linearity analysis, the IM3 is direct proportion to the second derivatives of the extrinsic transconductance (Gm″). The IP3 is an inverse proportion to Gm″ and direct proportion to third power of Gm. For this reason, the lower IM3 can be achieved by improving the Gm distribution flatness across the gate bias region. Meanwhile, higher Gm with flat Gm distribution also will result in higher IP3. In this paper, the extra doping either in the Schottky layer or in the channel layer was used to modify the drain-source current (I_{DS}) profile and to improve the Gm distribution flatness to improve device linearity.

7.3 Result and discussion

The three different types of InGaP/InGaAs HEMTs as shown in Fig.1 were fabricated, tested and compared. The device size was 0.25μm × 160μm. Figure7-2(a) shows the gate bias dependence of the Gm characteristics for these devices. It is observed that extra doping either in the channel or in the Schottky layer of the conventional δ doped InGaP/InGaAs PHEMT will result in more flat G_m distribution, but both have lower maximum Gm value as compared to the conventional δ doped device. The I_{DS}-V_{GS} curve comparison of these devices is shown in Figure7-2(b). It can be seen that the Schottky layer doped device results in higher I_{DSS} (I_{DS} @ V_{GS} = 0V), and the channel doped device has higher maximum I_{DS} value. The DC characteristics of these three 0.25 *u*m × 160 *u*m devices are compared in Table 7-1.

To further investigate the linearity performance of the three devices, polynomial curve fitting technique was applied on the transfer characteristic functions of these devices. Equation (9) was transformed to I_{DS}-V_{GS} curves that were expressed in terms of a high order polynomial as expressed in equation (2.17):

$$I_{DS}(V_{GS}) = A_0 + a_1 V_{GS} + a_2 V_{GS}^{\ 2} + a_3 V_{GS}^{\ 3} + a_4 V_{GS}^{\ 4} + a_5 V_{GS}^{\ 5} + \ldots.$$

Moreover, the IM3 levels incurred by the device can then be readily derived as equation (2.18) [5, 6]:

$$IM3 = \frac{3}{8} a_3 A^3 + \frac{50}{32} a_5 A^5$$

For a device with good linearity, I_{DS} should increase linearly with V_{GS}, therefore, a_1 should be larger and the higher order constants a_3 and a_5 should be minimized [6]. The coefficients of these devices extracted from the measurement data with V_{DS} = 1.5V are listed in Table I. Compare the data of these three different devices in Table I, it is clearly observed that channel doped device has larger a_1 and smaller a_3 and a_5

values, while Schottky layer doped device only shows lower a_3.

To evaluate the device linearity, IM3 and IP3 of these devices were measured. The IM3 and IP3 measurements were carried out by injecting two signals with the same amplitude but at two different frequencies: 5.8 GHz and 5.801GHz with the devices biased at V_{DS} = 1.5V, and adjust the I_{DS} to get the IP3 vs. I_{DS} curve. Figure7-3 shows the IP3 vs. I_{DS} curves of these three different 0.25 μm x 160 μm devices, the load impedance was firstly tuned for maximum power for each individual device. It shows that both devices with extra doping have higher IP3 value. The channel doped device has more wide high IP3 region versus different I_{DS}, but Schottky layer doped device has high IP3 in the lower I_{DS} DC bias region. The measured maximum IP3 of these devices are listed in Table II. The channel doped device shows higher IP3 of 21.02 dBm, higher Δ (IP3-P_{1dB}) of 14.23 dB, and higher IP3 to DC power consumption ratio (IP3/P_{DC}) of 4.97. Overall, the channel doped device has hghest value of figure of merit for device linearity. Figure7-4 shows the IM3 value of these three devices with DC bias point at maximum IP3 condition. Measured IM3 levels at 20dB backed off from P_{1dB} are also included in Table II. Much lower IM3 levels for the devices with extra doping are observed compared to the conventional δ doped device especially for the channel doped device (-82dBm). From the data in Figure7-2 to Figure7-4, it can be concluded that extra doping either in the channel region or in the Schottky layer can achieve flatter Gm distribution vs. V_{GS} bias and thus lower overall IM3 and higher IP3 of these devices even though the conventional δ doped device exhibits higher peak Gm.

The Gm distributions vs. different V_{DS} were also compared for these three different types of devices. Figure7-5 shows the Gm vs. V_{GS} distribution curves of these devices under different V_{DS} (Drain to source voltage) bias. For the Schottky layer doped device, Gm decreases with V_{DC} at higher V_{GS} bias, meanwhile for the

channel doped device, Gm increases with V_{DS} biases. Load pull measurement was performed on these devices with W-CDMA modulation signal as the input to evaluate the device linearity at different DC biases. P_{1dB}, gain and power-added efficiency (PAE) of these devices were measured by single tone input power at 5.8GHz and tuning the maximum power with different V_{DS} at class AB bias point, W-CDMA modulation signal was used as the input signal to meet the adjacent-channel power ratio (ACPR) with P_{1dB} at +/- 5 MHz offset and at +/- 10 MHz offset from the center frequency. Table7-3 summarizes the device power performance and the ACPR value. The channel doped device shows higher P_{1dB} with higher PAE. The correlation between the Gm profile and ACPR performance was studied. When the V_{DS} bias point increases, the adjacent-channel leakage power of the channel doped device and the Schottky layer doped device decreases and increases respectively. The δ doped InGaP/InGaAs PHEMT with lightly doping in the channel results in flatter the Gm distribution and the flatness of Gm distribution extended with increasing V_{DS} bias. Meanwhile for the Schottky layer doped device, the Gm flatness distribution compressed with increasing V_{DS} bias. The ACPR test for two these two devices by 5.8GHz W-CDMA modulation signal are shown in Figure7-6 with device V_{DS} bias at 3V. The channel doped device shows better power performance with P_{1dB} of 14.20 dBm, PAE of 29.23% and ACPR of -40 dBc at +/- 5 MHz offset and -55 dBc at +/- 10 MHz offset from the center frequency. Meanwhile for the Schottky layer doped device, the performance is inferior to the channel doped device with P_{1dB} of 11.47 dBm, PAE of 11.41% and ACPR of -21 dBc at +/- 5 MHz offset and -38 dBc at +/- 10 MHz offset were obtained. The channel doped device demonstrates much better linearity under CDMA modulation than the Schottky doped device especially at high V_{DS} bias condition.

7.4 Conclusions

The δ InGaP/InGaAs PHEMT with extra doping to improve the device linearity is demonstrated. The extra doping either in the channel layer or in the Schottky layer results in the improvement of the Gm vs. V_{GS} curve flatness and thus leads to lower overall IM3 and higher IP3 for these devices, even though the conventional device exhibits higher peak Gm. With the three different types of δ doped devices studied, the channel doped device with a light doping of $5\times10^{17}/cm^3$ in the channel region demonstrated highest maximum I_{DS} and flattest G_m versus V_{GS} curve and the Gm value of this device increases with increasing V_{DS} bias. These DC characteristics lead to higher IP3 levels and lower IM3 and the best ACPR under CDMA modulation for the channel doped device as compared to the other two types of devices studied even though it has the lowest electron mobility among these three devices. The experimental result in this work is consistent with the theoretical analysis. In summary, doping modification either in the channel region or in the Schottky layer is proven to be effective in improving the device linearity for the InGaP/InGaAs PHEMT devices in this study, this approach can be practically used for the development of high linearity devices for wireless communication applications.

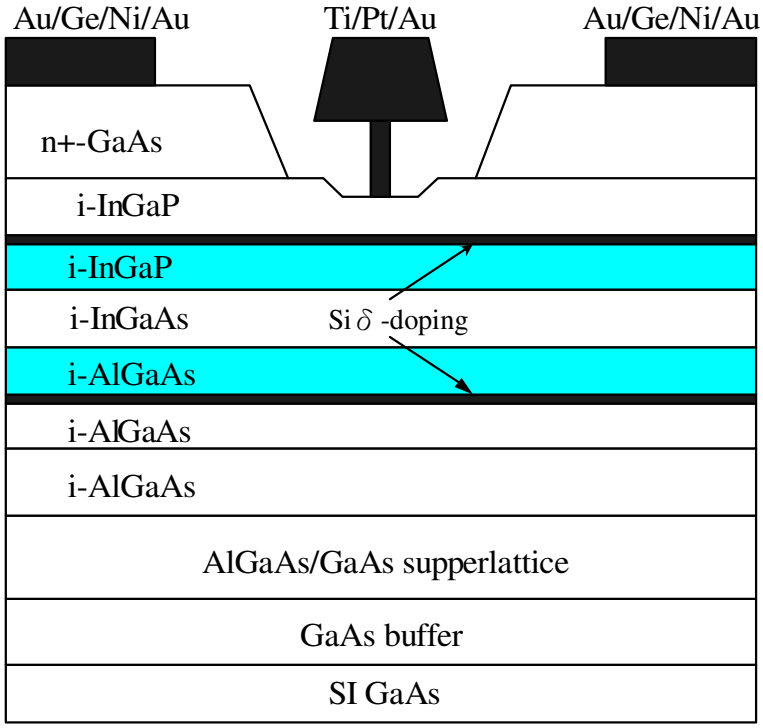

(a)

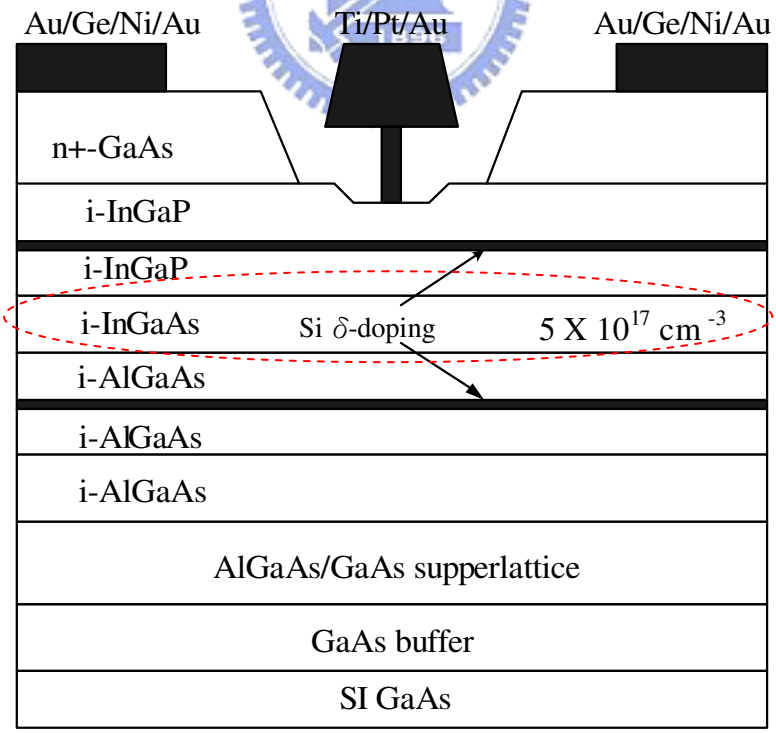

Figure7-1. Structures of the three InGaP/InGaAs PHEMTs in this study:(a) δ -doped device, (b) Channel doped PHEMT

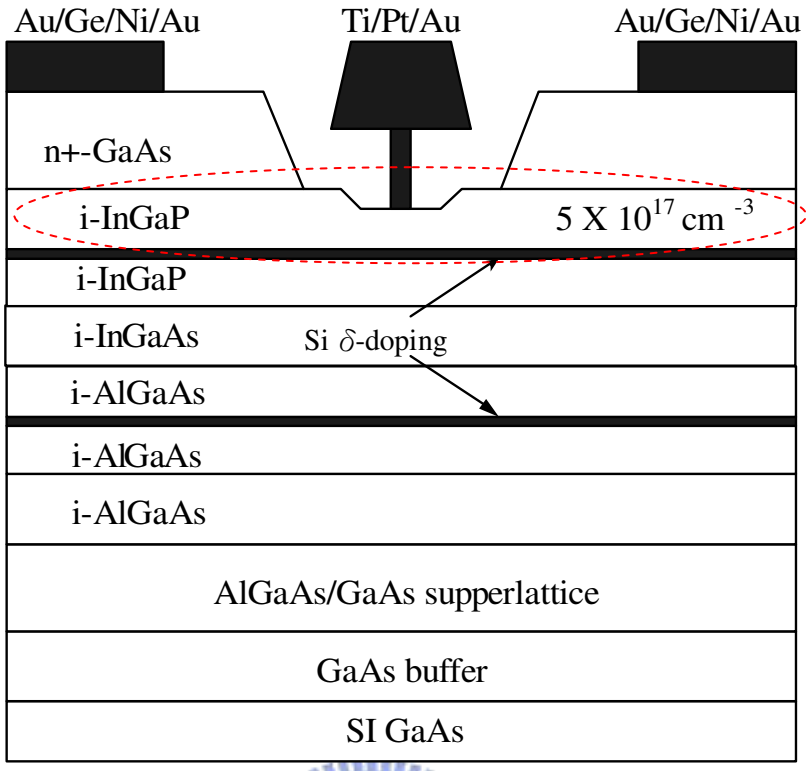

Figure7-1. Structures of the three InGaP/InGaAs PHEMTs in this study:

(c) Schottky layer doped

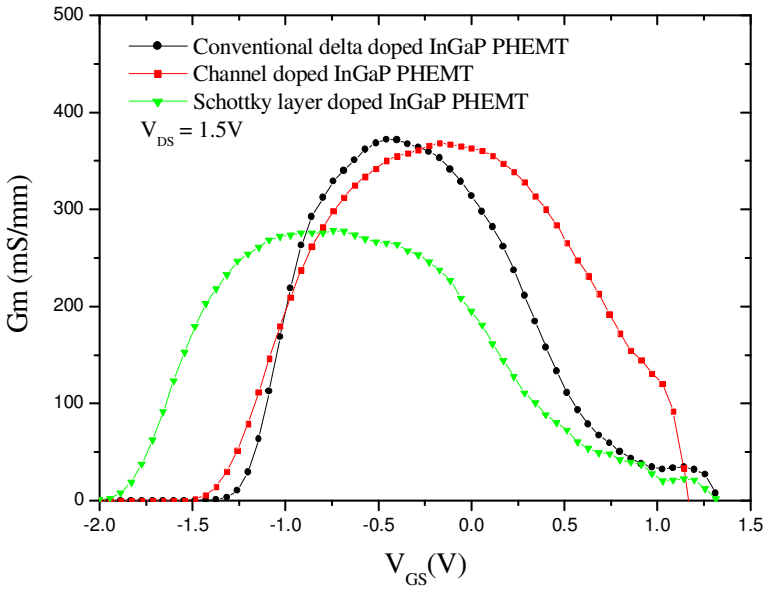

(a)

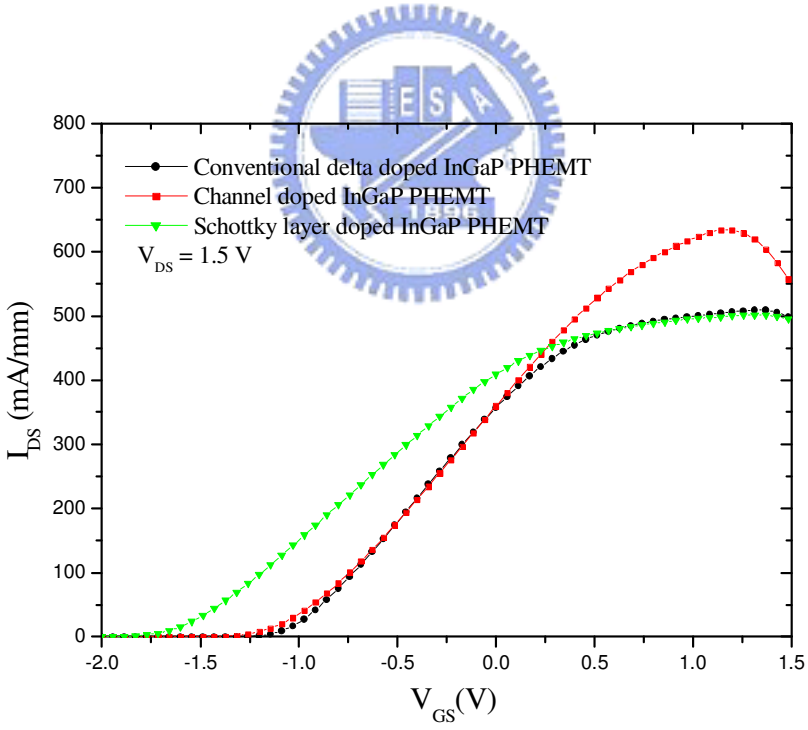

(b)

Figure7-2 (a) Extrinsic transconductance (G_m) vs V_{GS} curve, (b) I_{DS} vs V_{GS} curves for the three different types of devices studied, the device size is 0.25 x 160 μm^2 and the V_{DS} bias is 1.5V.

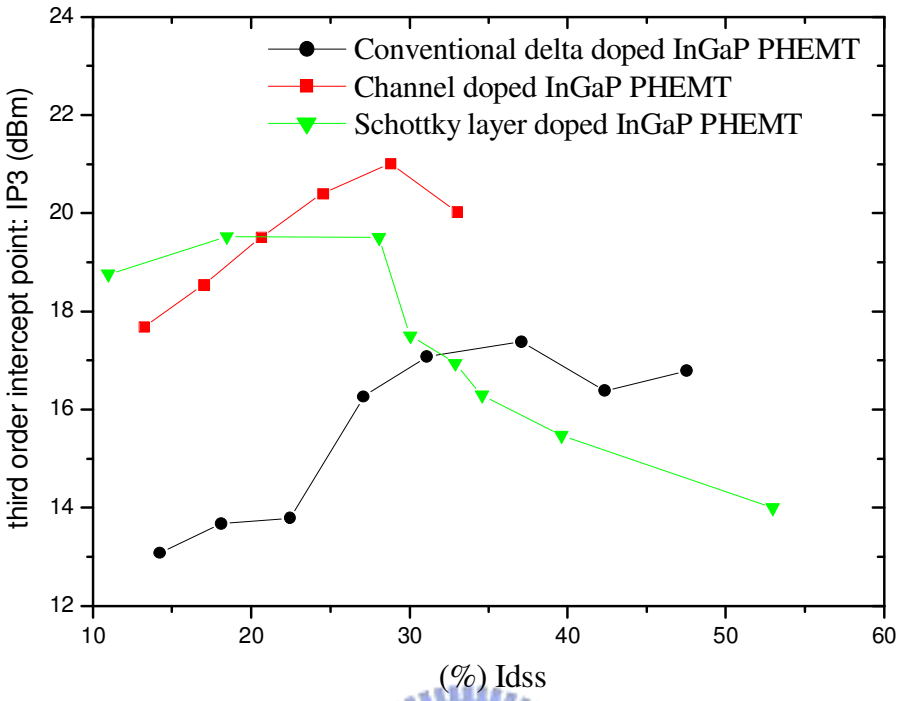

Figure7-3 IP3 vs. I_{DS} curves of the three 0.25x160 μ m^2 InGaP/InGaAs PHEMTs in this study, the test frequency is 5.8GHz and V_{DS} = 1.5V.

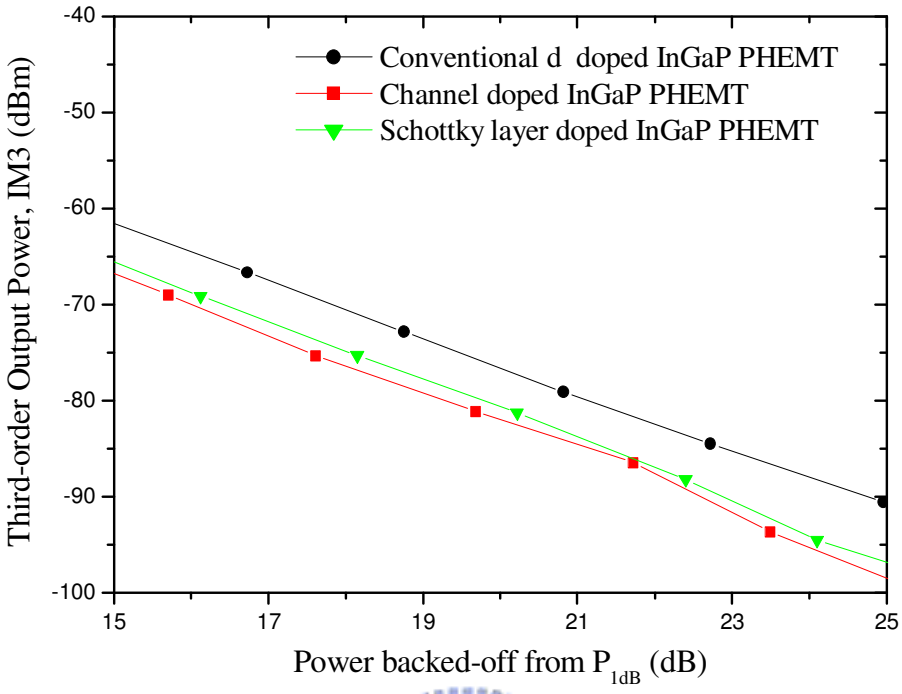

Figure7-4 IM3 vs. power backed off from P_{1dB} curves for the three different types of InGaP/InGaAs PHEMTs, device size: 0.25 x 160 μm^2, test condition: V_{DS}=1.5V, I_{DS} bias at maximum IP3 and the input signal frequency is 5.8GHz

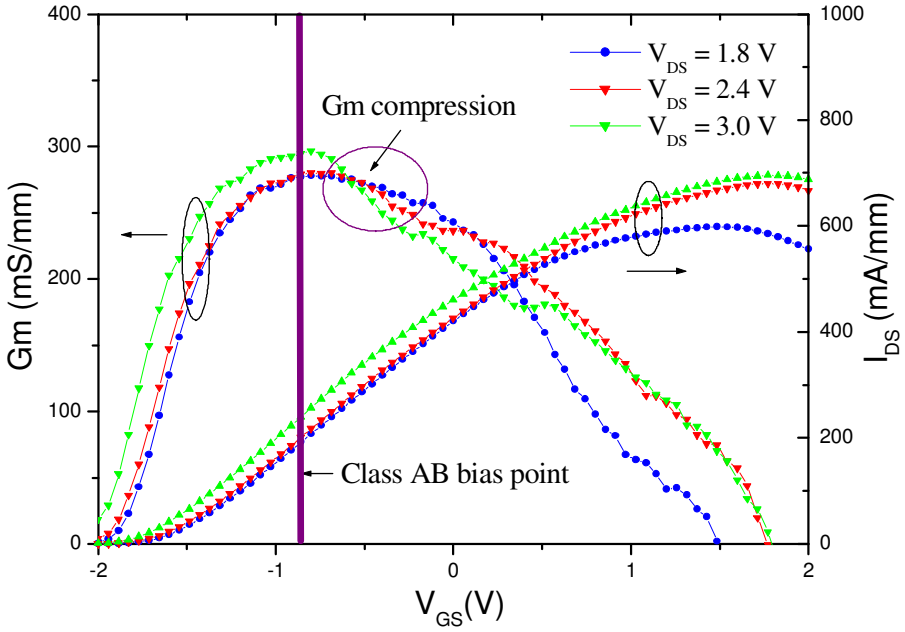

(a)

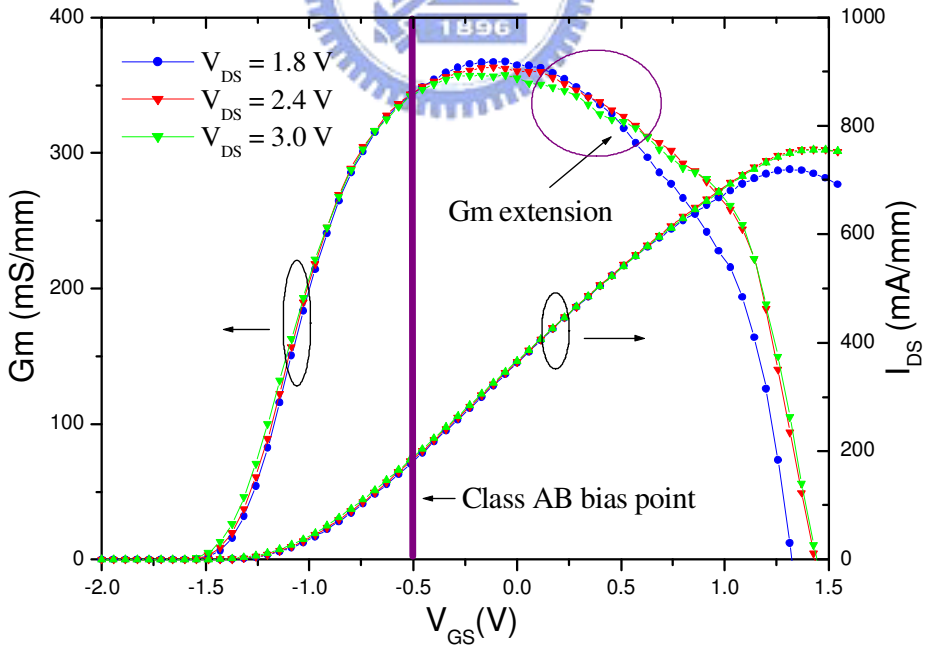

(b)

Figure7-5 Extrinsic transconductance (G_m) vs V_{GS} curves at different V_{DS} bias points for (a) The Schottky layer doped device, (b) The channel doped device.

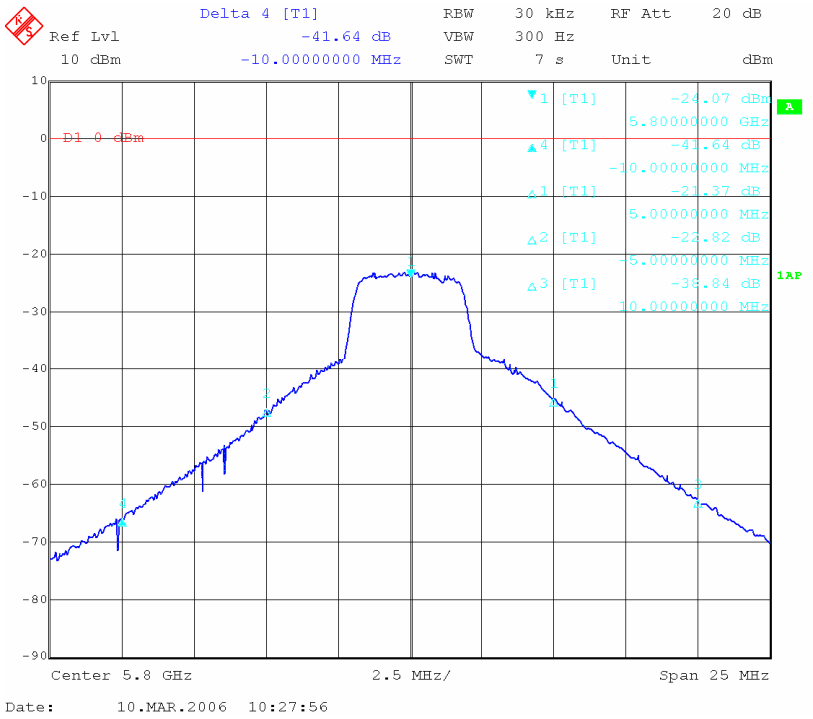

(a)

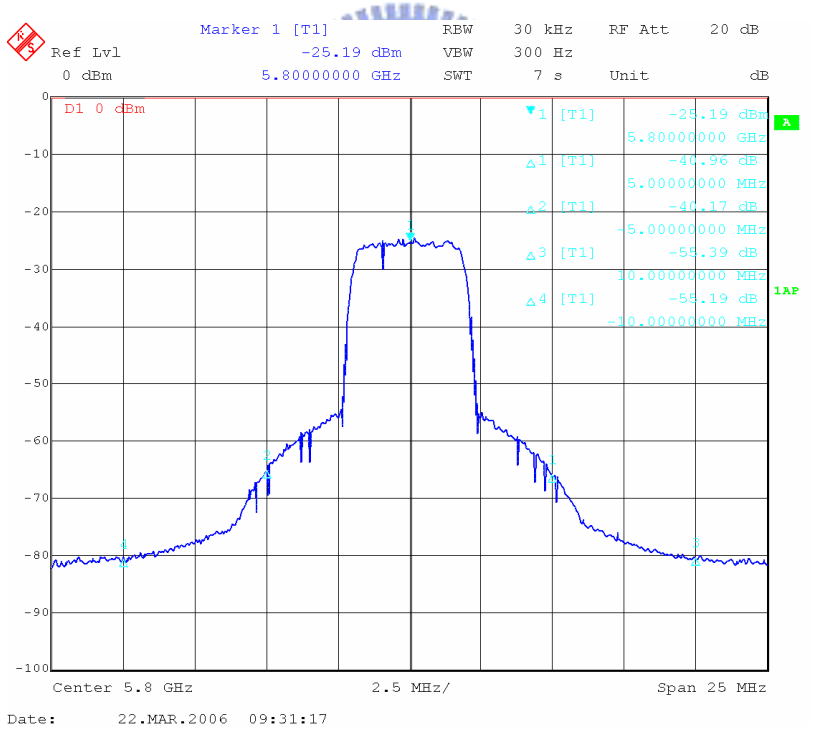

(b)

Figure7-6 ACPR spectrum of the InGaP/InGaAs PHEMTs (a) The Schottky layer doped device, (b) The channel doped device. (device size: 0.25 x 160 μm^2), test condition: V_{DS} = 3V, class AB bias and the input signal frequency is 5.8GHz.

Table7-1 Comparison of the DC characteristics of the three different types of devices.

Device Type			Conventional δ doped InGaP/InGaAs PHEMT	Schottky layer doped InGaP/InGaAs PHEMT	Channel doped InGaP/InGaAs PHEMT
Doping density	Delta doping (cm^{-2})	above	4.0×10^{12}	4.0×10^{12}	4.0×10^{12}
		below	2.0×10^{12}	2.0×10^{12}	2.0×10^{12}
	Channel layer(cm^{-3})		undoped	undoped	5.0×10^{17}
	Schottky layer(cm^{-3})		undoped	5.0×10^{17}	undoped
I_{DSS} (I_{DS} @ V_{GS}=0, mA/mm)			356.9	408.7	359.6
I_{DS}-max (mA/mm)			509.3	501.2	634.3
Gm_{max} (mS/mm)			372.1	277.6	368.4
Pinch-off voltage			-1.25	-1.80	-1.35
I_{DS}-V_{GS} polynomial 1st order coefficient a_1			0.04978	0.03079	0.05742
I_{DS}-V_{GS} polynomial 3rd order coefficient a_3			-0.01453	-0.00592	-0.00968
a_3 / a_1			-0.29188	-0.19227	-0.16858
I_{DS}-V_{GS} polynomial 5th order coefficient a_5			0.00385	0.00423	0.00015
a_5 / a_1			0.07734	0.13738	0.00261

Table7-2 Comparison of the IM3 and IP3 of the three different types of devices.

Device Type	DC bias point: V_{DS} = 1.5V					
		Operation frequency: 5.8GHz				
	I_{DS} (mA)	IM3 level at 20dB back-off from P_{1dB} (dBm)	P1dB (dBm)	IP3 (dBm)	Δ (IP3-P1dB) (dB)	IP3/P_{DC}
Conventional delta-doped InGaP/InGaAs PHEMT	22.34	-75	5.79	17.38	11.59	1.63
Schottky layer doped InGaP/InGaAs PHEMT	14.72	-80	5.43	19.52	14.10	4.06
Channel doped InGaP/InGaAs PHEMT	16.96	-82	6.79	21.02	14.23	4.97

Table7-3 P_{1dB}, Gain, PAE and ACPR of the three different devices under different V_{DS} at class AB bias.

Device	RF Performance		Class AB		
			V_{DS} =1.5	V_{DS} =2.4	V_{DS} =3.0
Schottky layer doped InGaP/InGaAs PHEMT	P1dB(dBm)		7.58	9.25	11.47
	Gain(dB)		20.11	21.98	22.49
	PAE(%)		9.55	8.76	11.41
	ACPR (dBc)	+5MHz offset	-28.75	-28.33	-21.37
		-5MHz offset	-30.19	-28.28	-22.82
		+10MHz offset	-47.28	-48.06	-38.84
		-10MHz offset	-51.20	-49.75	-41.64
Channel doped InGaP/InGaAs PHEMT	P1dB(dBm)		8.17	12.48	14.20
	Gain(dB)		13.63	13.89	14.01
	PAE(%)		15.08	25.43	29.23
	ACPR (dBc)	+5MHz offset	-32.30	-37.03	-40.96
		-5MHz offset	-32.43	-36.58	-40.17
		+10MHz offset	-51.40	-54.63	-55.39
		-10MHz offset	-53.05	-54.75	-55.19

Chapter 8

Conclusions

Theoretical base for achieving high linearity device is first discussed. The relationships between IM3 and IP3 with two current source Gm (V_{GS}) and Gds (V_{DS}) were derived. According to the linearity analysis in this study, the device linearity can be improved either by layer structure design or electron doping profile modification. Four different types of HEMT devices are studied based on the theoretical analysis in this study. They are: composite-channel MHEMT, uniformly doped MHEMT, InGaP/AlGaAs/InGaAs PHEMT, and δ doped InGaP PHEMT with doping channel and Schottky layer doping.

In the uniformly-doped $In_{0.52}Al_{0.48}As/In_{0.6}Ga_{0.4}As$ MHEMTs study, even though the δ doped device has higher peak transconductance, the uniformly-doped MHEMT shows much better device linearity. This is because the uniform doped device has more uniform electron distribution in the quantum well region which enables the device to possess straight I_{DS} versus V_{GS} curve and more flat G_m versus I_{DS} curve, and in turn results in much higher IP3 levels, higher Δ and higher IP3/P_{DC}. Thus, the uniformly-doped MHEMT device is more suitable than δ doped MHEMT for the modern digital wireless communication system application which impose very stringent linearity requirement for the devices.

For InGaP HEMT study, a novel InGaP/AlGaAs/InGaAs HEMT structure is proposed for the InGaP/AlGaAs/InGaAs PHEMT, the device shows very low noise figure, low third-order distortion, and low dc power consumption is developed. The outstanding performance of the device is attributed to the use of high band gap InGaP as the Schottky layer so as to improve the noise figure and reduce the gate leakage current, along with the use of AlGaAs as the spacer to improve the electron mobility,

and the use of dual delta doped layers to improve the device linearity. The developed InGaP/AlGaAs/InGaAs PHEMT with very low noise figure and leakage current and very high IP3 is of great use for the wireless communication applications.

In the δ doped InGaP/InGaAs PHEMT with extra doping study, the δ InGaP/InGaAs PHEMT with extra doping to improve the device linearity is demonstrated. The extra doping either in the channel layer or in the Schottky layer results in the improvement in the Gm vs. V_{GS} curve flatness and thus leads to lower overall IM3 and higher IP3 for the channel doped and Schottky layer doped devices even though the conventional device exhibits higher peak Gm. With the three different types of δ doped devices studied, the channel doped device with light doping $5\times 10^{17}/cm^3$ in the channel region demonstrated highest maximum I_{DS} and flattest G_m versus V_{GS} curve and the Gm value increases with increasing V_{DS} bias. These DC characteristics lead to higher IP3 levels and lower IM3 and the best ACPR under CDMA modulation for the channel doped device as compared to the other two types of devices studied even though it has lowest electron mobility among these three devices.

Overall, in this study, the experimental results in this work are consistent with the theoretical analysis. Layer structure design and doping modification either in channel region or in Schottky layer are proven to be effective in improving the device linearity for the HEMT devices in this study, this approach can be practically used for the development for high linearity devices for wireless communication application in the future.

REFERENCE

[1] Michael Jon Bailey, "Intermodulation Distortion in Pseudomorphic HEMT's and an Extension of the Classical Theory," IEEE TRANSACTIONS ON MICROWAVE THEORY AND TECHNIQUES, VOL. 48, NO. 1, pp. 104-110, JANUARY 2000.

[2] RODNEY S. TUCKER, "Third-Order Intermodulation Distortion and Gain Compression in GaAs FET's," IEEE TRANSACTIONS ON MICROWAVE THEORY AND TECHNIQUES, vol. MTT-27, no. 5, pp. 400-408, MAY 1979.

[3] H.Q. Zheng, G.I. Ng, Y.Q. Zhang, K. Radhakrishnan, K.Y. Lee, P.Y. Chee, M.S. Tse, J.X. Weng, and S.F. Yoon," High linearity, current drivability and fmax using pseudomorphic GaAs double -heterojunction HEMT (DHHEMT)', Semicond. Electron., pp.12-14,1996.

[4] Yi-Ien Chan and Ming-Ta Yang, "Device Linearity Improvement by $Al_{0.3}Ga_{0.7}As/In_{0.2}Ga_{0.8}As$ Heterostructure Doped-Channel FET's," IEEE ELECTRON DEVICE LETTERS, VOL. 16, NO. 1, pp. 33-35, JANUARY 1995.

[5] K.Y. Hur, K.T. Hetzler, R.A. McTaggart, D.W. Vye, P.J. Lwmonias and W.E. Hoke, "Ultralinear double pulse doped AlInAs/GalnAs/lnP HEMTs," ELECTRONICS LETTERS, Vol. 32, No. 16, pp. 1516 – 15181, Aug. 1996.

[6] ANDREA M.CROSMUN, and STEPHEN A. MAAS, "Minimization of Intermodulation Distortion in GaAs MESFET Small-Signal Amplifiers," IEEE TRANSACTIONS ON MICROWAVE THEORY AND TECHNIQUES, VOL. 37, NO. 9, pp. 1411-1417, SEPTEMBER 1989.

[7] José Carlos Pedro and Jorge Perez, "Accurate Simulation of GaAs MESFET's Intermodulation Distortion Using a New Drain-Source Current Model," IEEE TRANSACTIONS ON MICROWAVE THEORY AND TECHNIQUES, VOL. 42, NO. 1, pp. 25-33, JANUARY 1994.

[8] Nuno Borges de Carvalho, and José Carlos Pedro, “Large- and Small-Signal IMD Behavior of Microwave Power Amplifiers,” IEEE TRANSACTIONS ON MICROWAVE THEORY AND TECHNIQUES, VOL. 47, NO. 12, pp. 2364-2374, DECEMBER 1999.

[9] Hsien-ChinChiu, Shin-Cheng Yang, Feng-Tso Chien, and Yi-Jen Chan, “Improved Device Linearity of AlGaAs/InGaAs HFETs by a second Mesa Etching,” IEEE ELECTRON DEVICE LETTERS, VOL. 23, NO. 1, JANUARY 2002.

[10] S.R. Bahl, M.H. Leary, and J.A. del Alamo, ”Mesa-sidewall gate leakage in InAlAs/InGaAs heterostructure filed-effect transistors,” IEEE Trans. Electron. Devices, Vol. 39, Issue 9, pp. 2037-2043, Sept. 1992.

[11] Y. Okamoto, K. Matsunaga, M. Kuzuhara, and M. Kanamori, ” Novel InGaP/AlGaAs/InGaAs heterojunction FET for X-Ku band power applications,” IEEE MTT-S Int. Microw. Symp. Dig., 1997, 3, pp. 1191-1194.

[12] C. Gaquiere, F. Bue, P. Delemotte, Y. Crosnier, B. Carnez and D. Pons, “Effects on the Linearity in Ka Band of Single or Double-Recessed PHEMT’s,” IEEE MICROWAVE AND GUIDED WAVE LETTERS, VOL. 10, NO. 7, pp. 267- 269, JULY 2000.

[13] K. Onda, A. Fujihara, A. Wakejima, E. Mizuki, T. Nakayama, H. Miyamoto, Y. Ando, and M. Kanamori,” InAlAs/InGaAs channel composition modulated transistors with InAs channel and AlAs/InAs superlattice barrier layer,” IEEE ELECTRON DEVICE LETTERS, VOL. 19, NO 8, pp. 300-302, AUGUST 1998.

[14] M.S. Heins, J.M. Carroll, M. Kao, J. Delaney, and C.F. Campbell, “X-band GaAs mHEMT LNAs with 0.5dB Noise Figure,” IEEE MTT-S Digest, pp. 149-152, 2004.

[15] C.S. Whelan, W.E. Hoke, R.A. McTaggart, S.M. Lardizabal, P.S. Lyman, P.F. Marsh, and T.E. Kazior, "Low Noise $In_{0.32}(AlGa)_{0.68}As/In_{0.43}Ga_{0.57}As$ Metamorphic HEMT on GaAs Substrate with 850 mW/mm Output Power Density," IEEE ELECTRON DEVICE LETTERS, VOL. 21, NO. 1, pp. 5-8, JANUARY 2000.

[16] Colin S. Whelan, Phil F. Marsh, William E. Hoke, Rebecca A. Mc Taggart, Peter S. Lyman, Peter J. Lemonias, Steven M. Lardizabal, Robert E. Leoni III, Steven J. Lichwala, and Thomas E. Kazior, "Millimeter-Wave Low-Noise and High-Power Metamorphic HEMT Amplifiers and Devices on GaAs Substrates," IEEE JOURNAL OF SOLID-STATE CIRCUITS, VOL. 35, NO. 9, pp. 1307-1311, SEPTEMBER 2000.

[17] Edward Yi Chang, Yueh-chin Lin, Guan-Ji Chen, Huang-Ming Lee, Guo-Wei Huang, D. Biswas, and Chun-Yen Chang, "Composite-Channel Metamorphic High Electron Mobility Transistor for Low-Noise and High-Linearity Applications," JJAP, Vol. 43, No. 7A, pp. L871-L872, 2004.

[18] Feng-Tso Chien and Yi-Jen Chan, "Improved AlGaAs/InGaAs HFETs due to double doped-channel design," ELECTRONICS LETTERS, Vol. 35, No. 5, pp. 427-428, 4th March 1999.

[19] E. Lan, E. Johnson, B. Knappenberger, and M. Miller, "InGaP PHEMTs for 3.5GHz W-CDMA applications," IEEE MTT-S Digest, vol. 2, pp.1039-1042, 2-7 June 2002.

[20] Ming-Yih Kao, Edward A. Beam III, Paul Saunier, and Willian R. Frensley, "X-BAND InGaP PHEMTs WITH 70% POWER-ADDED EFFICIENCY," IEEE MTT-S Digest, vol. 3, pp.1671-1674, 7-12 June 1998.

[21] Y. C. Lin, E. Y. Chang, G. J. Chen, H. M. Lee, G. W. Huang, D. Biswas and C. Y. Chang,"InGaP/InGaAs PHEMT with high IP3 for low noise applications,"

ELECTRONICS LETTERS, vol. 40, no. 11, pp. 777-778, 10 June 2004.

[22] P. PAUL RUDEN, MICHAEL SHUR, AKINTUNDE I. AKINWANDE, JAMES C. NOHAVA, DAVID E. GRIDER, and JUNHO BAEK, “AlGaAs/InGaAs/GaAs Quantum Well Doped Channel Heterostructure Field Effect Transistors,” IEEE TRANSACTIONS ON ELECTRON DEVICES, VOL. 37, NO. 10, pp. 2171-2175, OCTOBER 1990.